

GDOT Research Project 14-14

FINAL REPORT

**Travel-time Optimization on I-285 with
Improved Variable Speed Limit Algorithms and
Coordination with Ramp Metering Operations**



**OFFICE OF PERFORMANCE-BASED MANAGEMENT AND RESEARCH
15 KENNEDY DRIVE
FOREST PARK, GA 30297-2534**

1. Report No. FHWA-GA-19-1414		2. Government Accession No.		3. Recipient's Catalog No.	
4. Title and Subtitle Travel-time Optimization on I-285 with Improved Variable Speed Limit Algorithms and Coordination with Ramp Metering Operations				5. Report Date February, 2019	
				6. Performing Organization Code	
7. Author(s) Jorge A. Laval, Ph.D., Angshuman Guin, Ph.D., Bhargava Chilukuri, Ph.D., and Hyun W. Cho				8. Performing Organization Report No. 14-14	
9. Performing Organization Name and Address School of Civil and Environmental Engineering Georgia Institute of Technology 790 Atlantic Dr. Atlanta, GA 30332-0355				10. Work Unit No. (TR AIS)	
				11. Contract or Grant No. PI# 0013186	
12. Sponsoring Agency Name and Address Office of Performance-based Management and Research 15 Kennedy Dr Forest Park, GA 30297-2534				13. Type of Report and Period Covered November 2014 – February 2019	
				14. Sponsoring Agency Code	
15. Supplementary Notes Prepared to the Georgia Department of Transportation					
16. Abstract The objective of this project is to develop effective variable speed limit (VSL) control algorithms to minimize the total travel time on I-285 study corridor. The study corridor is Eastbound/Southbound I-285 between GA 400 and I-20. Using a stochastic simulation-based optimization framework that combines microsimulation model GTsim and a genetic algorithm-based optimization module, we determine the optimal parameter values of a combined variable speed limit and ramp metering (VSL-RM) system that minimizes total vehicle travel time. The total travel time is reduced by 8% compared to no control.					
17. Key Words Variable Speed Limit, Ramp Metering, Genetic Algorithm Optimization				18. Distribution Statement	
19. Security Classif. (of report) Unclassified	20. Security Classif. (of this page) Unclassified		21. No. of pages 82	22. Price	

Form DOT F 1700.7 (8-72) Reproduction of completed page authorized

Table of Contents

1	Introduction.....	1
2	Literature Review.....	3
2.1.	Variable Speed Limit	3
2.1.1.	Theoretical background	4
2.1.2.	Variable Speed Limit Algorithm	9
2.1.3.	Variable Speed Limit and Ramp Metering	11
3.	Variable Speed Limit Systems.....	17
3.1.	GDOT Variable Speed Limit Systems	17
3.1.1.	Simulation of the GDOT speed harmonized VSL	20
3.2.	Combined Variable Speed Limit-Ramp Metering Algorithm at Merge Bottleneck.....	24
3.2.1.	Problem Formulation	24
3.3.	Model	26
3.3.1.	Preventing capacity drop using VSL	26
3.3.2.	Combined VSL and RM Model.....	31
4.	Optimization Framework	39

4.1.	GTsim Application.....	39
4.2.	Genetic Algorithm.....	40
5.	Methodology.....	41
5.1.	Study corridor.....	41
5.2.	Traffic Data Analysis	43
5.2.1.	Data.....	43
5.2.2.	Data Processing for Origin Destination Matrix Estimation.....	48
5.2.3.	Calibration and Validation.....	54
6.	Results.....	57
7.	Conclusions.....	63
8.	References.....	65
9.	Appendix.....	73

List of Figures

Figure	Page
1. (a) Potential VSL impact on under-critical mean speed and (b) cross-point of diagrams with and without VSL.	4
2. Four phases of the SPECIALIST algorithm	5
3. VSL strategy for a steady queue	7
4. Discretized motorway link	8
5. Example of the rule-based VSL algorithm	9
6. Rolling horizon system and control algorithm.....	10
7. ALINEA: local ramp metering strategy.....	11
8. Two examples for increase in on-ramp flow and decrease in mainline freeway flow during a queue flush.....	13
9. Persistent flow control via VSL.....	14
10. (a) PI-ALINEA (feedback RM); (b) RM network; (c) feedback VSL; (d) VSL network; (e) feedback integrated control (RM and VSL); (f) RM and VSL integrated network.....	15
11. Time-space diagrams of point (P) and section (S) VSL applications.....	16
12. GDOT NaviGator VSL system.....	18
13. Map of the VSL 21 and connected VDS's.....	18

14. GDOT NaviGator VSL map	19
15. Example network of speed harmonization (VSL)	21
16. (a) The continuous speed reduction of VSL #21 and (b) Speed contour map of harmonized speed algorithm shown as a time-space diagram.....	22
17. Isolated bottleneck at a merge area	25
18. Capacity drop at a merge area	25
19. Newell-Daganzo merge model	26
20. VSL upstream of the merge area	27
21. Fundamental mainline diagram and the time-space diagram representation of a strategy for eliminating on-ramp queue.....	27
22. Cumulative count curves of the capacity drop and VSL	30
23. Time-space diagram of the metering rate during the void period.....	33
24. Time-space diagram of the recovery of the capacity drop using the integrated RM and VSL model for mainline traffic.....	35
25. Cumulative count curve of Figure 23 and Figure 24.	36
26. Study Corridor	41
27. GDOT NaviGator video detection system (VDS)	45
28. Locations of GDOT NaviGator's Vehicle Detection System (blue) and Variable speed limit (red) on Google Map.	46

29. GDOT traffic tube counts	47
30. Flow chart of O/D matrix estimation	48
31. Sample network for OD estimation	49
32. O/D matrix	53
33. (a) Time Space Speed map of NaviGator (field data) (b) Time Space Speed map of GTsim (simulation).....	56
34. Speed contour map of the no control case	58
35. Speed contour map of the RM only control case.....	59
36. Speed contour map of the VSL-RM control case.	60
37. Typical Traffic State on I-285 Corridor on Monday PM Peak.....	73
38. Typical Traffic State on I-285 Corridor on Tuesday PM Peak.....	74
39. Typical Traffic State on I-285 Corridor on Wednesday PM Peak.....	75
40. Typical Traffic State on I-285 Corridor on Thursday PM Peak	76
41. Typical Traffic State on I-285 Corridor on Friday PM Peak.....	77
42. April 2016 Monday Traffic.....	78
43. April 2016 Tuesday Traffic.	79
44. April 2016 Wednesday Traffic.	80
45. April 2016 Thursday Traffic.....	81
46. April 2016 Friday Traffic.....	82

List of Tables

Table	Page
1. GDOT VSL lookup table (unit: mph).....	17
2. Sample O/D calculation table	50
3. Sample calculated and observed flow.....	51
4. Flow calculation.....	52
5. Calibrated Parameters	54
6. Travel time (vehicle hours) comparison of no control, the RM control only, the VSL-RM control cases, and the current GDOT's VSL control.....	57
7. Optimal parameter values of the RM only and VSL-RM models	62

EXECUTIVE SUMMARY

The objective of this project is to develop effective Variable Speed Limit (VSL) control algorithms to minimize the total travel time on EB/SB I-285 study corridor between GA-400 and US-78. This objective was accomplished with a simulation-based optimization framework using the *GTsim* microsimulation application, which allows us to optimize the coordinated operation of VSL control with the existing ramp metering (RM) control, and to forecast travel times to improve the efficiency of VSL control. Extensive traffic data for the study corridor were collected and processed for calibration.

We found that the current GDOT VSL algorithm is unable to improve travel times, even using the optimal parameters found in this project. The main reason is that the current algorithm was designed in order to harmonize the speed of traffic flow, which is the standard approach worldwide. However, this approach has not been shown to improve freeway capacity, and the travel time savings reported in the literature (~5-10%) come from incident reductions.

We propose a new combined VSL-RM algorithm designed to maximize freeway capacity by avoiding the capacity drop phenomenon at merge bottlenecks. It is found that the new algorithm is effective in preventing a capacity drop in that the ensuing travel time savings are significant compared to the ramp-metering-only option. The optimal speed of the VSL-RM algorithm was formulated from shock wave theory and experimented using *GTsim*.

This study analyzed extensive traffic data to generate origin-destination (O-D) flows of the study corridor. We used tube counters (flow) data for on- and off- ramps and

NaviGator (flow and speed) data for the mainline freeway to estimate travel times for each O-D. This study also developed GA-based optimization method to generate optimal parameters of the proposed VSL-RM algorithm. We found that the proposed VSL-RM algorithm reduces the total travel time by 8% compared to no control and 15% compared to GDOT's current algorithm.

From the analysis and results of this study, we recommend GDOT to revise the current VSL algorithm to incorporate other traffic features (density, flow, and capacity) so that the proposed VSL-RM can contribute improving capacity of the freeway and reducing travel time. Then, the B/C ratio of the updated system can be assessed with standard methods but based on this study we estimate that it should be in the range of 200:1 due to the low implementation cost.

1 Introduction

Since a ramp metering system was empirically proved to be effective in improving capacity and safety of mainline freeway (Mizuta, Roberts, Jacobson, & Thompson, 2014), the Georgia Department of Transportation (GDOT) had installed more than 160 ramp metering systems in metro Atlanta freeways in 2017. Previously, GDOT used a time-of-day ramp metering algorithm, where metering rates are predetermined from historical traffic data. Recently, GDOT adopted ALINEA for their new ramp metering algorithm, which is real-time density-based algorithm, and they also implemented a queue flush algorithm to prevent queues from backing up to the city streets. However, parameters of these algorithms are temporal and location specific, and need to be determined cautiously.

In 2014, to improve safety and relieve congestion, GDOT implemented variable speed limits (VSL) on the northern half of I-285, known as the most congested corridors of metro Atlanta. GDOT's VSLs are operated in real-time, and as the main purpose of VSL is to improve safety, speed limits are determined by harmonizing speeds. Although VSL has been touted as an effective tool to improve traffic flow, there is currently no solid empirical or scientific evidence that current harmonizing algorithm can relieve congestion.

The objective of this project is to develop effective VSL control algorithms to minimize the total travel time on EB/SB I-285 study corridor between GA-400 and US-78. This objective is accomplished with a simulation-based optimization framework using the GTsim microsimulation application, which allows us to optimize the

coordinated operation of VSL control with the existing ramp metering control, and to forecast travel times to improve the efficiency of VSL control.

2 Literature Review

This chapter presents a literature review of the effects of VSL on traffic flow, research methodologies on VSL such as the kinematic wave model, capacity drops, simulation modeling, and traffic control.

2.1. Variable Speed Limit

To the best of our knowledge, the earliest VSL systems were proposed by Smulders (1990), who aimed to homogenize and stabilize traffic to improve flow and safety. Subsequent studies presented the effectiveness of VSL in terms of the enhancement of safety and the reduction of accidents (Abdel-Aty, Cunningham, Gayah, & Hsia, 2009; Abdel-Aty, Dilmore, & Dhindsa, 2006; Lee, Hellinga, & Saccomanno, 2006), the efficiency of traffic flow (Bertini, Boice, & Bogenberger, 2006; Markos Papageorgiou, Kosmatopoulos, & Papamichail, 2008), and reductions of shock waves (Hegyi, De Schutter, & Hellendoorn, 2005b; Hegyi, Hoogendoorn, Schreuder, Stoelhorst, & Viti, 2008). Recent studies have suggested that combining VSL and ramp metering or near future technology such as connected vehicles (CV) would reinforce the benefits of the VSL system (Chen & Ahn, 2015; Han, Chen, & Ahn, 2017; Khondaker & Kattan, 2015a). Notice that this project does not assume the presence of automated vehicles.

2.1.1. Theoretical background

2.1.1.1 Effects of VSL on traffic flow

Papageorgiou et al. (2008) studied the impact of VSL on traffic flow characteristics and presented a fundamental diagram, shown in Figure 1. They found changes in both the slope and the critical occupancy. Considering that the VSL algorithm that they used was an imperfect rule-based algorithm, their findings still shed light on future research on the effectiveness of VSL on traffic flow.

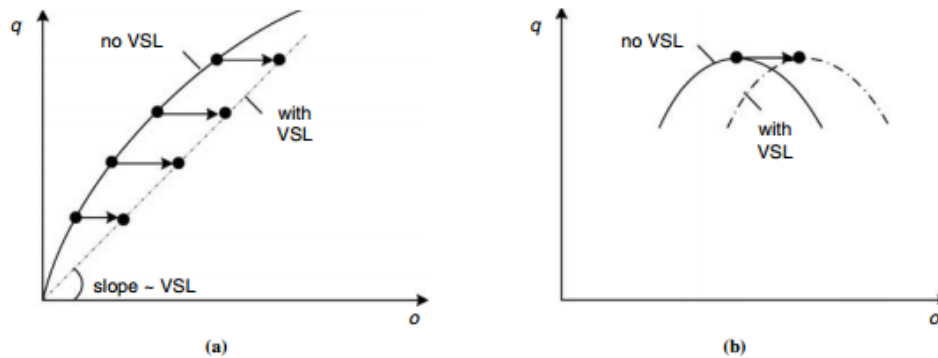


Figure 1 (a) Potential VSL impact on under-critical mean speed and (b) cross-point of diagrams with and without VSL (Markos Papageorgiou et al., 2008). q is the flow (vehicles/hr) and o is the occupancy (%).

Recent studies have empirically discovered the relationship between VSL and lane flow distribution (LFD) or traffic flow characteristics between lanes (Duret, Ahn, & Buisson, 2012; Knoop, Duret, Buisson, & Van Arem, 2010; Soriguera, Martinez, Sala, & Menendez, 2017). From empirical data, Duret (2014), Duret et al. (2012), and Knoop et al. (2010) showed that VSL homogenizes the speed between lanes so that shoulder lanes can be used; Soriguera et al. (2017), however, presented evidence that it may not reduce

the flow of the mainline, and for moderate demand, lower speed limits increase speed differences across lanes, thus increasing the incidence of lane-changing.

2.1.1.2 Kinematic Wave Theory and VSL

Several studies have explained the effectiveness of the VSL system by kinematic (shock) wave theory (Chen & Ahn, 2015; Chen, Ahn, & Hegyi, 2014; Hadiuzzaman & Qiu, 2013; Han et al., 2017; Hegyi & Hoogendoorn, 2010; Hegyi et al., 2008; H. Y. Jin & Jin, 2015; Schelling, Hegyi, & Hoogendoorn, 2011; Yang & Rakha, 2017). The earliest proposed VSL algorithm based on shock wave theory was SPECIALIST (SPEEd Controlling ALgorithm using Shock wave Theory), a method of resolving the moving jams (Figure 2). In the figure, when the VSL system detects a shock wave (state 2 in the figure), the VSL is on upstream of the shock wave (state 3) and then relaxes the VSL to the higher speed limit (states 4, 5) to the following vehicles. As a result, the shock wave is not propagated upstream. Later, this research was extended to recurrent and non-recurrent bottlenecks situations.

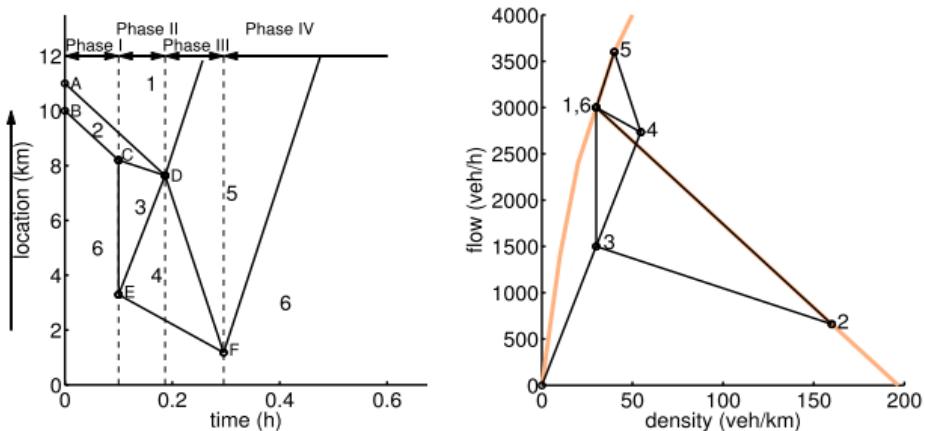


Figure 2 Four phases of the SPECIALIST algorithm (Hegyi & Hoogendoorn, 2010)

2.1.1.3 Capacity drop and VSL

Although Hadiuzzaman and Qiu (2013) and Hadiuzzaman, Qiu, and Lu (2012) proposed a cell transmission model (CTM) (Daganzo, 1995)-based analytical model to understand the effectiveness of VSL control that incorporates capacity drops, this study did not explain the mechanism of VSL as the solution of the capacity drop.

As noted in (Yang & Rakha, 2017), two VSL pioneer studies presented the mechanism of the capacity drop at bottlenecks and VSL as a solution. Jin and Jin (2013) presented a VSL control strategy based on a proportional-integral (PI) controller to effectively mitigate traffic congestion (the capacity drop) and reduce travel time at a lane-drop bottleneck. In their study, the VSL regulated the upstream inflow, and the authors used a controller to maintain stability in a zone between the VSL zone and the lane-drop bottleneck, which prevented a capacity drop.

Several studies proposed VSL control for fixed and non-recurrent freeway bottlenecks (Chen & Ahn, 2015; Chen et al., 2014; Han et al., 2017) and further developed it using connected vehicles. These studies, basing VSL strategies on the kinematic wave theory, starve inflow to the bottleneck to dissipate the upstream queue (see Figure 3). After clearing the queue, the VSL continues to regulate inflow to the bottleneck, maximizing the discharge rate and preventing a capacity drop.

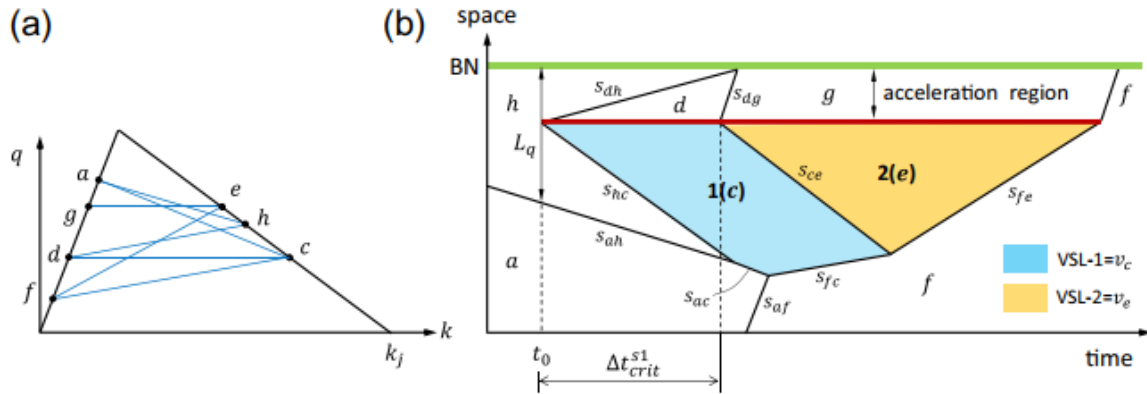


Figure 3 VSL strategy for a steady queue: (a) FD with VSL, and (b) a time-space diagram of VSL

(Chen et al., 2014). **q** is the flow (vehicles/hr) and **k** is the vehicle density (vehicles/km).

Recently, Yang & Rakha (2017) proposed a bang-bang feedback VSL (i.e., speed harmonization) algorithm that controls the mainline freeway to prevent or delay a capacity drop. By using a microscopic simulation, this study demonstrated their algorithm and showed an increase in the bottleneck discharge rate and reductions in emissions and fuel consumption.

2.1.1.4 Simulation Modeling of VSL

For safety reasons, directly implementing traffic flow models in the real world is difficult without prior scrutiny. The most popular methods of proving the effectiveness of traffic flow models are simulation modeling and experiments. Simulation methods of traffic can be categorized into micro and macro simulation. Researchers who have studied the safety benefits of VSL used off-the-shelf micro-simulation software such as VISSIM or PARAMICS (Abdel-Aty et al., 2006; Abdel-Aty, Pande, Lee, Gayah, & Dos Santos, 2007; Lee et al., 2006). Other researchers who presented the traffic flow efficiency of VSL used the macroscopic traffic flow model (e.g., the cell transmission model,

METANET (see Figure 4) (Carlson, Papamichail, & Papageorgiou, 2011, 2014; Carlson, Papamichail, Papageorgiou, & Messmer, 2010b; Hadiuzzaman et al., 2012; Hegyi, De Schutter, & Hellendoorn, 2005a; Hegyi et al., 2005b; Lu, Qiu, Varaiya, Horowitz, & Shladover, 2010)).

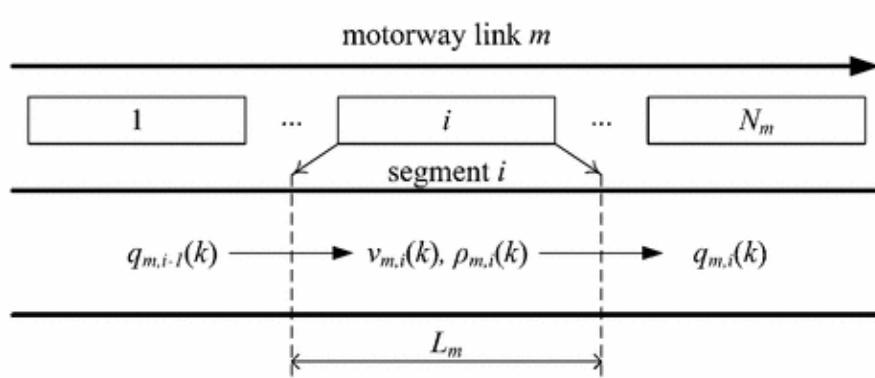


Figure 4 Discretized motorway link (Carlson et al., 2010b)

2.1.2. Variable Speed Limit Algorithm

2.1.2.1. Rule-based Algorithm

VSL algorithms can be classified into reactive rule-based or proactive algorithms. The rule-based algorithm determines the speed limit based on traffic coefficients: speed, flow, density (occupancy) threshold (see Figure 5) (Allaby, Hellinga, & Bullock, 2007; Chang, Park, & Paracha, 2011; Kang, Chang, & Zou, 2004; Lin, Kang, & Chang, 2004; Talebpour, Mahmassani, & Hamdar, 2013). The main objective of such VSL systems is to harmonize the speed between upstream and downstream (vertically) traffic or lanes (laterally). Studies have shown that rule-based algorithms are effective at harmonizing traffic and improving safety; their efficiency to improve traffic flow and travel time savings is arguable (Khondaker & Kattan, 2015b).

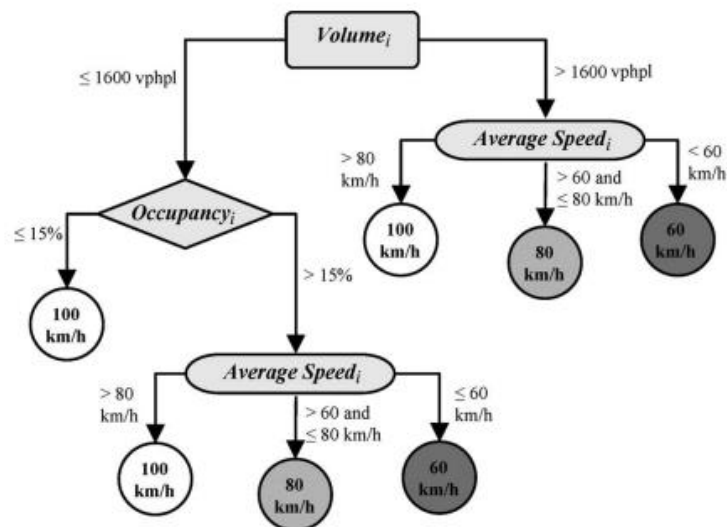


Figure 5 Example of the rule-based VSL algorithm (Allaby et al., 2007)

For the rule-based algorithm, setting conservative threshold values might reduce the risk of a crash, but it would exacerbate traffic congestion. Also, because of the time

lag between current traffic and future controlled traffic, if incautious threshold values were chosen, future traffic could not take advantage of the VSL system (Khondaker & Kattan, 2015b). It is also worth mentioning that the location of VSLs and durations or update periods of the control of VSLs are important factors related to the effectiveness of a rule-based VSL algorithm.

2.1.2.2. Proactive Algorithm

The proactive algorithm, which does not have the limitations of the rule-based algorithm, adopts a rolling horizon system (see Figure 6), control theory approaches, and a METANET model, all of which have been explained in previous studies (Fang, Hadiuzzaman, Karim, Luo, & Qiu, 2014; Hadiuzzaman et al., 2012; Hegyi et al., 2005a; Lu, Qiu, et al., 2010; Lu, Varaiya, Horowitz, Su, & Shladover, 2010). For example, Model Predictive Control (MPC) predicts future traffic based on traffic state and control input and computes optimal control values (speed limits). METANET, used in MPC modeling, discretizes distance and time so that it can easily calculate the optimal location and time period of the VSL system. However, the MPC approach, probably because of its complexity, has not been implemented in the real world.

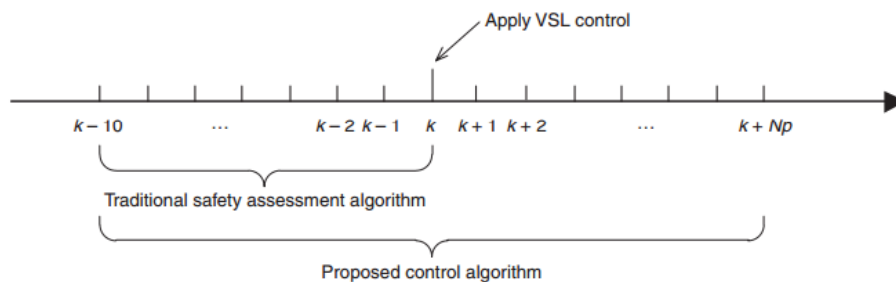


Figure 6 Rolling horizon system and control algorithm (Fang et al., 2014)

2.1.3. Variable Speed Limit and Ramp Metering

2.1.3.1. Ramp Metering ALINEA

Ramp metering (RM) has been shown to be effective at increasing mainstream outflow by controlling the inflow of on-ramps. The most popular algorithm of ramp metering is ALINEA, a local feedback strategy that calculates metering rates $r(t)$ using past time-step metering rates $r(t - \Delta t)$ and differences between current and target occupancy ($\hat{o} - o_{out}(t)$) (M. Papageorgiou, Hadj-Salem, & Middelham, 1997) (see equation (1), Figure 7).

$$r(t) = r(t - \Delta t) + K_R(\hat{o} - o_{out}(t)) \quad (1)$$

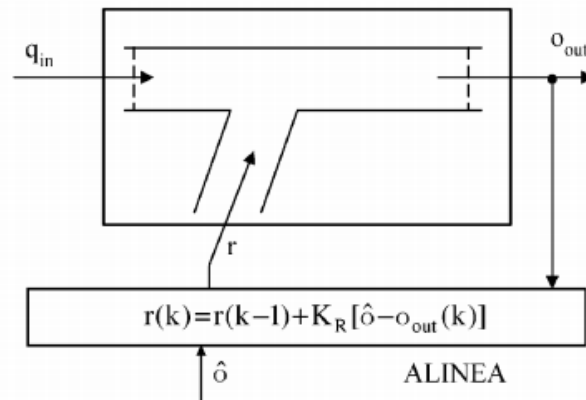


Figure 7 ALINEA: local ramp metering strategy (Markos Papageorgiou & Kotsialos, 2002)

2.1.3.2. *Queue Flush in Ramp Metering*

A restrictive metering rate of an on-ramp induces a queue to spill back to the upstream arterial road. To prevent this situation from occurring, queue flush systems are a common solution (Bhargava R Chilukuri, Laval, & Chen, 2013; Bhargava Rama Chilukuri, 2015), which turns off the ramp meter signal when a loop detector installed at the end of the queue storage detects a queue spillback. Chilukuri et al. (2013) found that although a queue flush resolves the queue of the on-ramp, it decreases flow on the mainline freeway (see Figure 8). The queue flush algorithm consists of maximum and minimum density thresholds (k_{max} , k_{min}) of loop detectors and the number of data collecting time periods (n), shown in the following equation.

$$k_{max} \geq \frac{\sum_{i=1}^n k_i}{n}$$

$$k_{min} \leq \frac{\sum_{i=1}^n k_i}{n}$$

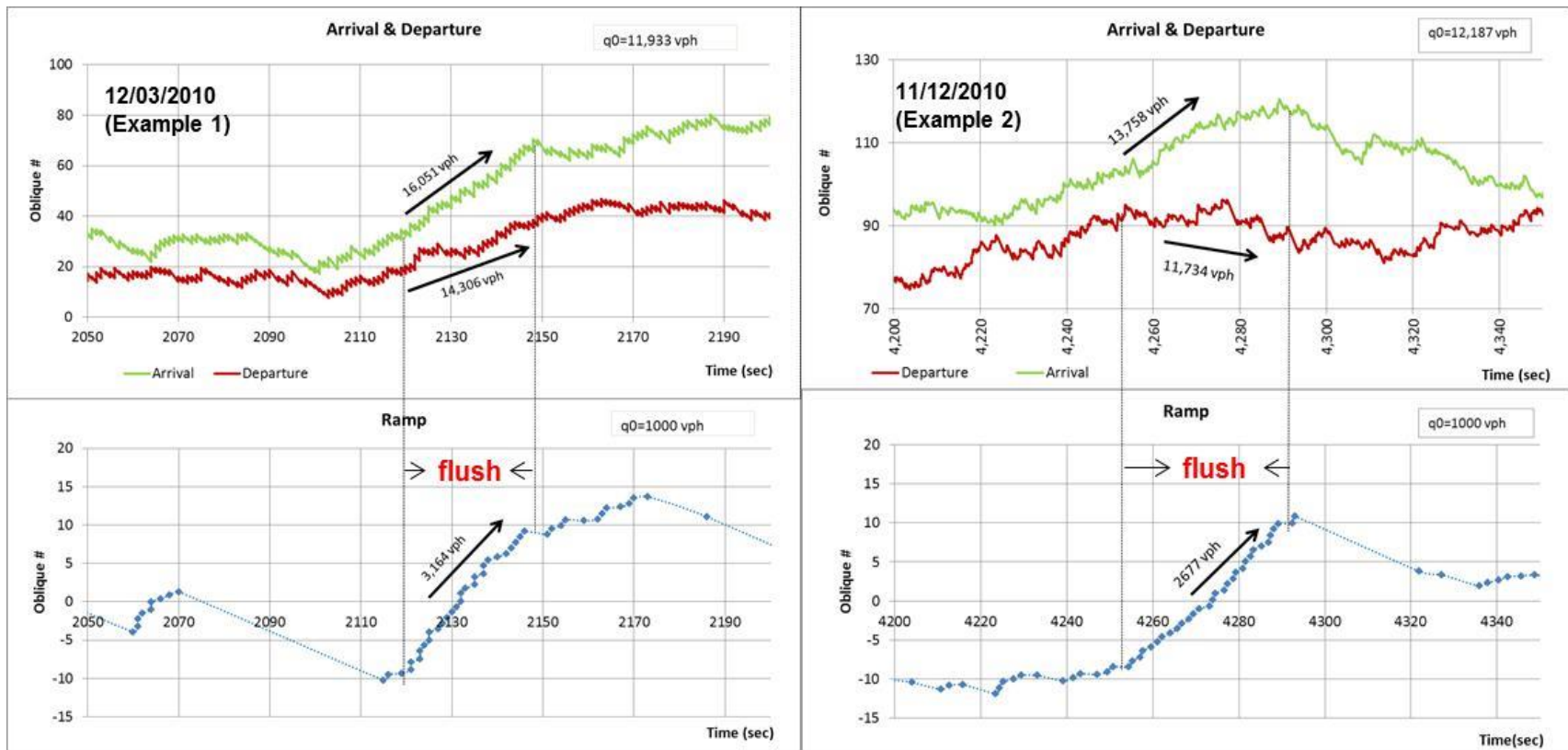


Figure 8 Two examples for increase in on-ramp flow and decrease in mainline freeway flow during a queue flush

(a) 12/03/2010 (left column) (b) 11/12/2010 (right column) (Bhargava R Chilukuri et al., 2013)

2.1.3.3. VSL and RM Integrated System

The research group that developed the ALINEA control strategy proposed to use the VSL as a RM (Carlson et al., 2010b). In their work, VSL decreases the mainstream flow to the potential bottleneck segment, resulting in delaying bottleneck activation at under-critical occupancies (Figure 9). Their assumption of the impact of VSLs on traffic flow is based on empirical data (Markos Papageorgiou et al., 2008).

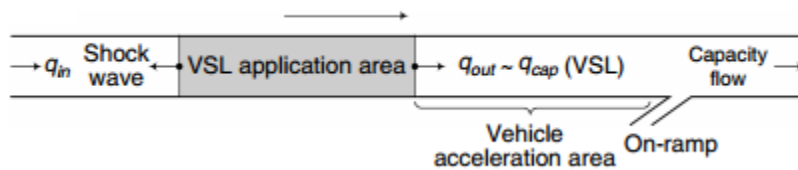


Figure 9 Persistent flow control via VSL (Carlson et al., 2010b)

Assuming that the VSL acts as a RM, the research team proposed the integrated optimal control system on the VSL/RM combined network using the METANET traffic flow model and expressed the VSL impact as $v(k) = v^* b_m(k)$, where $b_m(k)$ is the magnitude of speed limits ($b_m(k) < 1$). The main objective of the control is to find the minimum total time spent, considering VSL magnitude $b_m(k)$, the ramp queue length, and traffic oscillation costs. After comparing the results of four scenarios—No-Control, Coordinated Ramp Metering, VSL Control, and VSL and RM Integrated Control—they showed that integrated control surpasses other cases and further tested their system on large-scale networks (Carlson, Papamichail, Papageorgiou, & Messmer, 2010a).

Despite the outstanding simulation results from the previous work, the VSL and RM integrated control based on the optimal control method encountered challenges in

practical applications because of the limitations and restrictions related to practical traffic systems. To overcome these challenges, Carlson et al. (2011, 2014) further proposed a feedback-based VSL and RM control in which traffic flow modeling and systems objectives were the same as those of the previous work, but instead of optimal control, they chose feedback-based control (Figure 10).

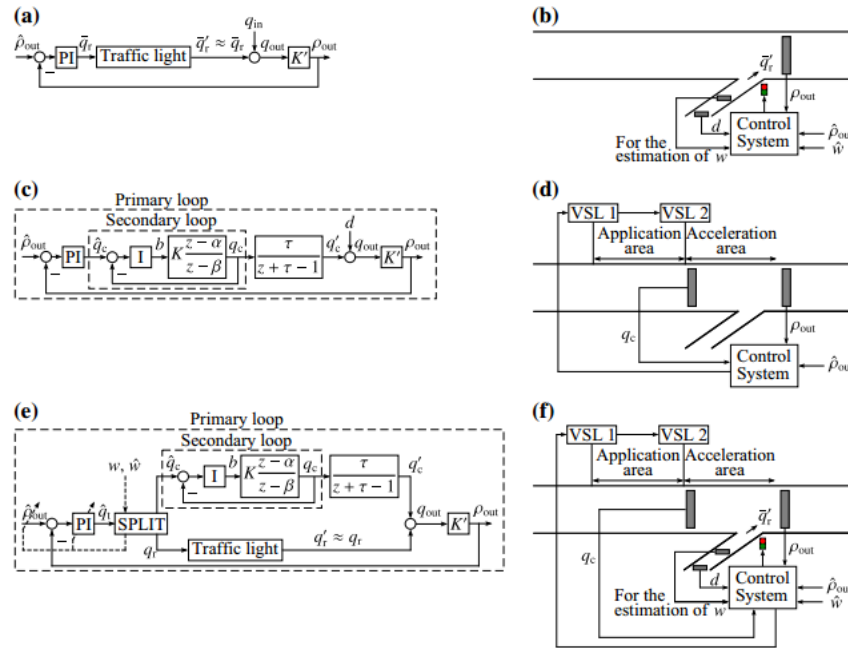


Figure 10 (a) PI-ALINEA (feedback RM); (b) RM network; (c) feedback VSL; (d) VSL network; (e) feedback integrated control (RM and VSL); (f) RM and VSL integrated network (Carlson et al., 2014).

Using METANET, the team tested the feedback-based model and compared it to optimal control and several other scenarios. They found that the integrated feedback-based model saves close to the same amount of total travel time as the optimal control model. Although the feedback-based model is not superior to the optimal control model regarding achievements of the objectives, the authors reported that the feedback-based

model is applicable in the real world because it does not use an online model or demand predictions. However, until now, field tests of the strategy have not been conducted. Therefore, to support the practical aspects of VSL, Müller, Carlson, Kraus, and Papageorgiou (2015) proposed a micro-simulation analysis of VSL using AIMSUN. In their research, they implemented a VSL system similar to the real-world environment, such as ways of applying section-level VSL or point-level VSL, the length of the application area, and the length of the acceleration area (Figure 11). They concluded that section-VSL is preferable to point-VSL, and that the shorter application and acceleration areas decrease delay.

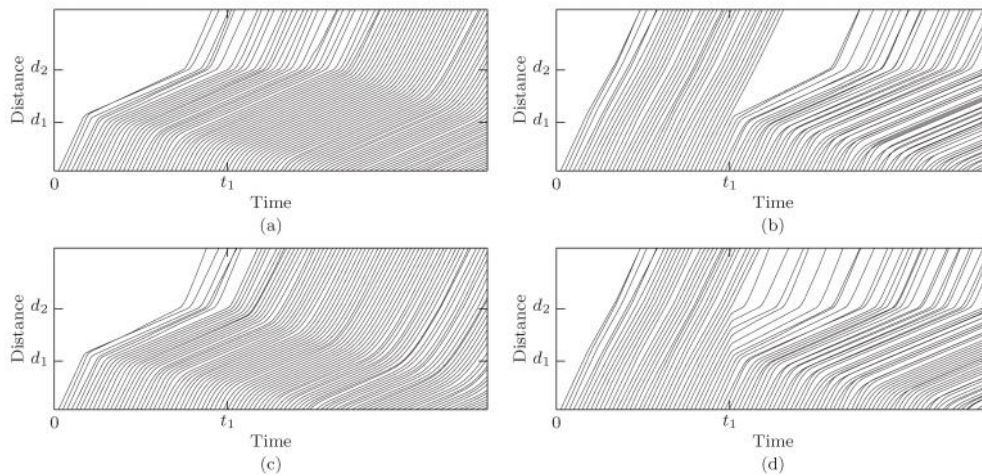


Figure 11 Time-space diagrams of point (P) and section (S) VSL applications. (a) P-VSL increase; (b) P-decrease; (c) S-VSL increase; and (d) S-VSL decrease (Müller et al., 2015)

3. Variable Speed Limit Systems

3.1. *GDOT Variable Speed Limit Systems*

GDOT adopted speed harmonization as their VSL algorithm. According to the algorithm, each VSL of the corridor is connected to adjacent GDOT NaviGator's Vehicle Detection System (VDSs). The number of these VDSs and their locations vary by VSL. Figure 12 depicts the VSL #21 screenshot of the GDOT NaviGator System. This figure shows that GDOT-VSL-021 is connected to VDSs, GDOT-STN-2850026, 27, 28, 29. Figure 13 shows the exact location of the VSL and VDSs. Note that GDOT-STN-2850027, 28, 29 are VDS 2818, 19, 20 in Figure 13, and GDOT-STN-2850026 (VDS 2817) is not working. VDS's collect the average speed of vehicles that pass the location every 20 seconds, and the VSL system calculates the average number of cycles and the average speed of the VDS's. The calculated VSL speed then refers to Table 1 to determine the displayed speed limit. The VSL algorithm has a constraint that the differences among the display speed limit of adjacent VSLs should not be more than 10 *mph*. Figure 14 GDOT NaviGator VSL map shows the VSL map of the GDOT NaviGator system.

Table 1 GDOT VSL lookup table (unit: mph)

Low Limit (\geq)	High Limit ($<$)	Display Speed Limit
59	100	65
47	59	55
35	47	45
1	36	35

Viewer 55 GDOT-VSL-021: I-285 E @ 27.9 Last Polled: 2017-06-05 15:59:15

VSL ID	GDOT-VSL-021	
Location	I-285 E @ 27.9	
Group	Clockwise 21	
Status	OK	OK
Downstream Speed	64	
Troop Speed	66	
Current Mode	Harmonization	
User	djansen	
Mode ends at	2017-06-11 23:00:00	
Selected SL	65	
Constrained by	Downstream Reduce	
Recommended SL	55	
Recommended at	2017-06-05 16:01:52	
Posted at	2017-06-05 15:59:15	
Durable until	-	
Current Posted SL	55	55
Last refresh at	06-05 15:59:15	06-05 15:59:09
Expires at	06-05 16:13:53	06-05 16:13:53
Lag	22 sec	16 sec
Sign Errors	No Errors	No Errors

US DS

STATUS **SCHEDULE**

VDS	Use	Dist	Timestamp	Spd	Avg Speed	Cycles	Good Cycles
GDOT-STN-2850026	<input checked="" type="checkbox"/>	01.21	NA	NA	NA	0	0
GDOT-STN-2850027	<input checked="" type="checkbox"/>	01.63	16:01:40	65	65	6	6
GDOT-STN-2850028	<input checked="" type="checkbox"/>	02.12	16:01:40	66	65	6	6
GDOT-STN-2850029	<input checked="" type="checkbox"/>	02.59	16:01:40	56	63	6	6

DMS Location

DMS CCTV Events VDS Beacons RACS Gate VSL LCS HERO Signals

Figure 12 GDOT NaviGator VSL system

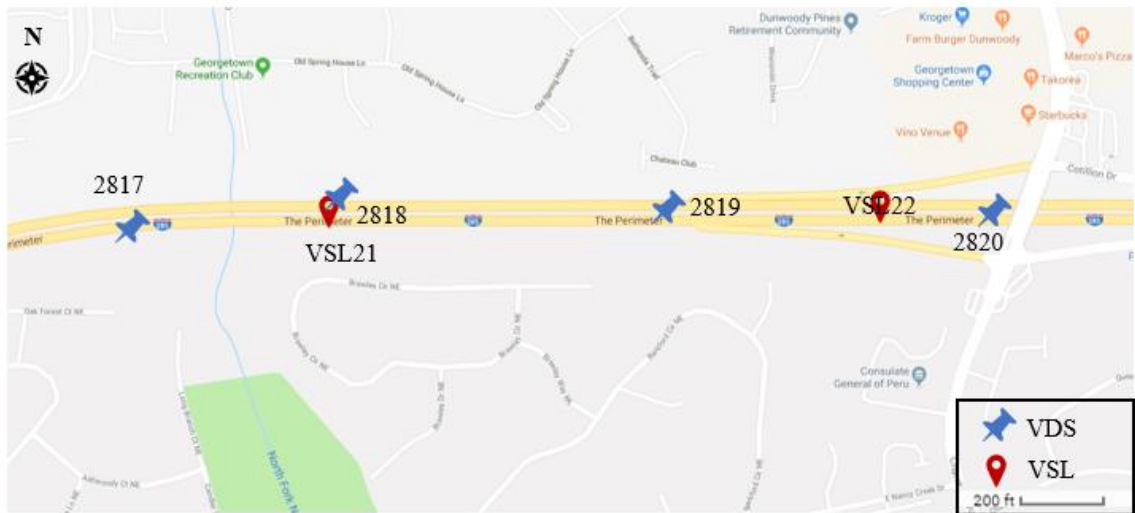


Figure 13 Map of the VSL 21 (upstream of Chamblee Dunwoody Rd) and connected VDS's

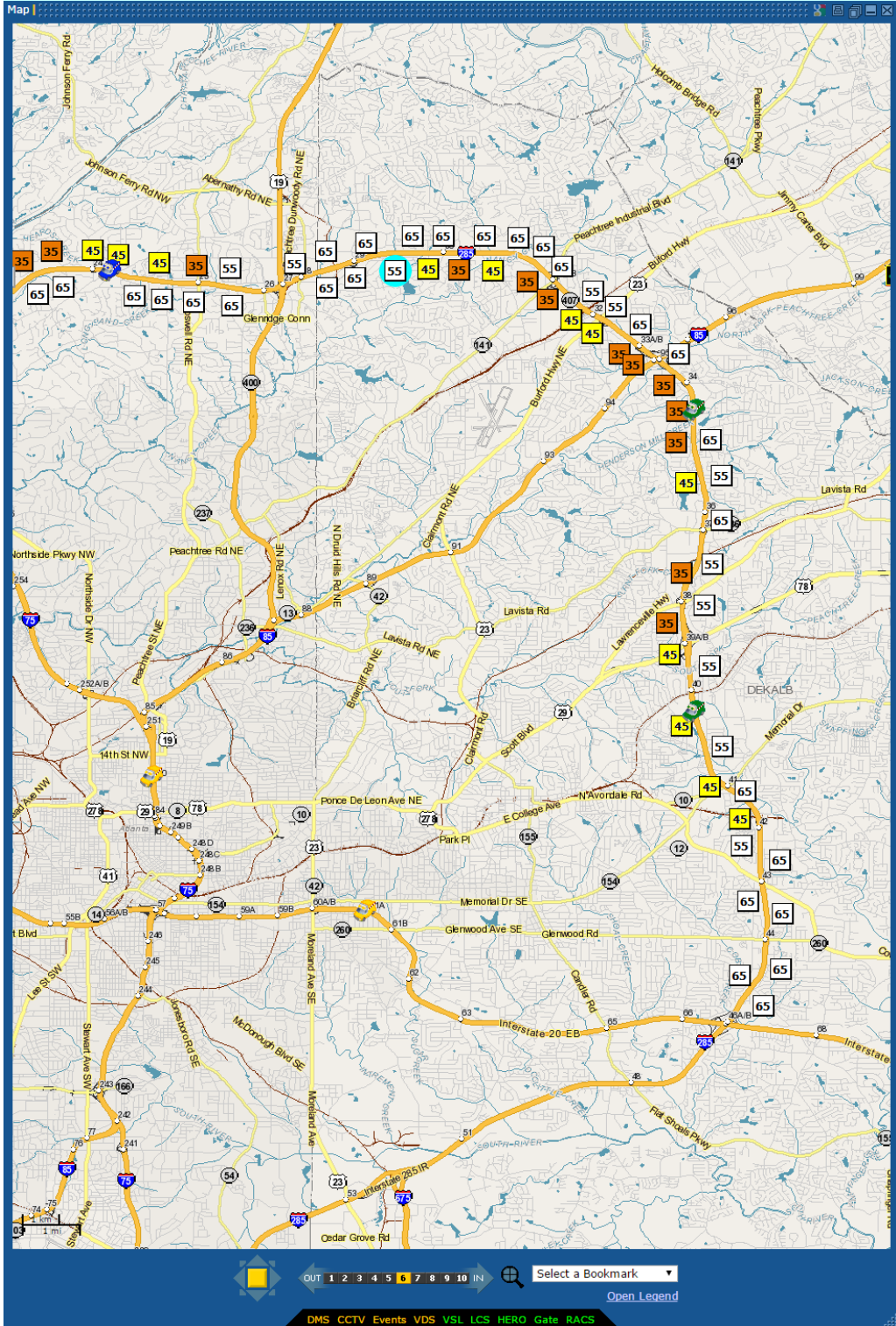


Figure 14 GDOT Navigator VSL map

3.1.1. Simulation of the GDOT speed harmonized VSL

We explained that the VSL algorithm harmonizes speeds upstream and downstream of a particular VSL display. Some studies (Abdel-Aty et al. (2009, 2007)) have shown the effectiveness of speed harmonization from a safety perspective with microscopic traffic simulations. These studies proposed a crash risk index that includes rear-end and lane-change crash risk and measured changes in the index in various environments. However, as the objective of this study is to reduce congestion on the study corridor using the RM and the VSL, the safety perspective is beyond the scope of this study. Although many studies (Carlson et al. (2014, 2010a); Hegyi et al. (2005a)) have proven the effectiveness of VSL using the macroscopic traffic model, to the best of our knowledge, very few studies (Talebpour et al. (2013)) have proven the effectiveness of speed harmonization in terms of reducing congestion (saving travel time) with microscopic simulation.

In this simulation study, which is based on the real world replicated in the study corridor and data, modeling an efficient speed harmonization VSL model was particularly difficult. The main reason is that VSL and VDS locations are prefixed, and they do not account for the formation of bottlenecks in certain locations. As shown next, these limitations can produce undesirable results when driver compliance is 100 percent. Consider the example network in Figure 15. In the Figure, VSL1 is connected to VDS 1, 2, 3 and that a VSL 2 is connected to VDS 4, 5, 6. Notice that it is not uncommon that some VDSs in our study corridor are located upstream of the VSL. The bottleneck of this network is located between the VDS3 and the VDS 4. When the bottleneck becomes activated, the queue backs up upstream, and VDS 3, 2, 1 detects the congested speed of

vehicles in an orderly manner, and the VSL₁ shows the harmonized speed. If we assume a vehicle passes the VSL signage in strict compliance with the VSL, the vehicle will not increase speed to free-flow even if it passes the bottleneck. In this case, the VDS 4 detects the decreased speed of the vehicle, and the VSL 2, which shows the harmonized speed of VDS 4, 5, and 6, will post the decreased speed because of the decreased speed of the VDS 4 even if the bottleneck is not detected downstream of the VSL 2. As the decreased speed of the VSL 2 is the maximum speed of the vehicle which passes the VSL 2, this results in a new unexpected bottleneck. After this new bottleneck activates, it worsens the upstream traffic as a queue from this bottleneck propagates upstream, which results in the speed of the VSL 1 continuously decreasing.

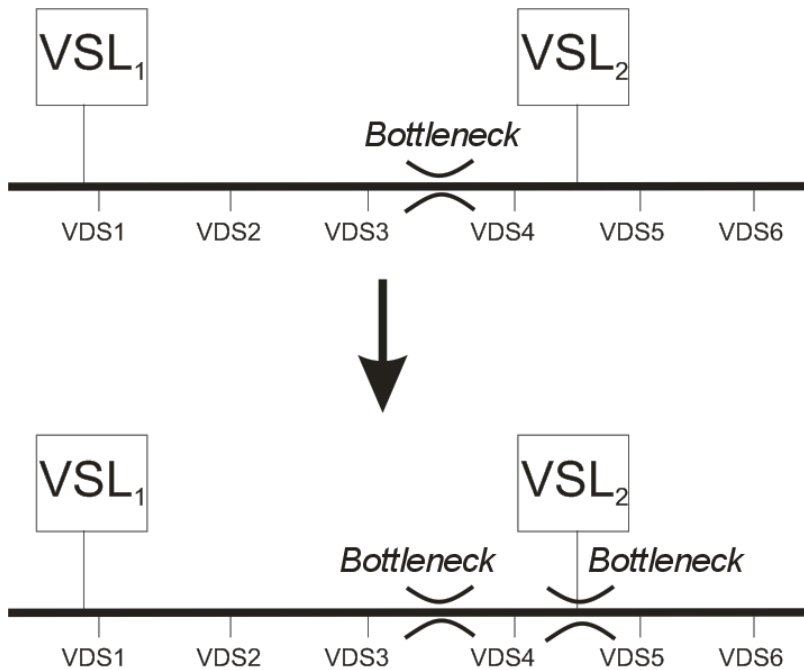
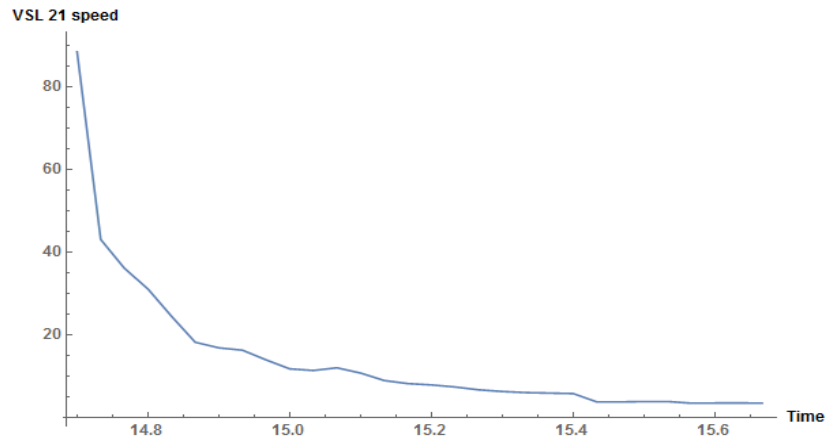
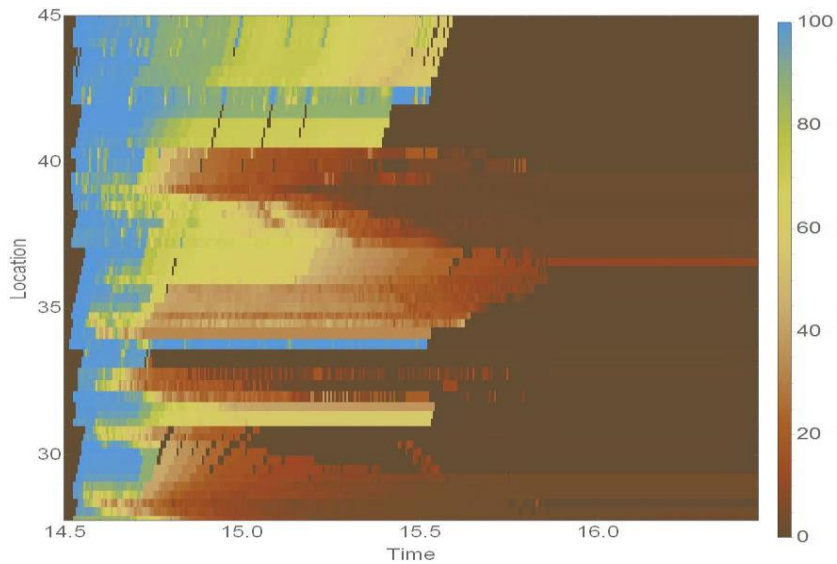


Figure 15 Example network of speed harmonization (VSL)

This phenomenon was found after the research team implemented GDOT's speed harmonization algorithm in GTsim. Figure 16 shows an example of the speed of the VSL and a speed contour map of GTsim.



(a) Speed of VSL #21



(b) Speed contour map

Figure 16 (a) The continuous speed reduction of VSL #21 and (b) Speed contour map of harmonized speed algorithm shown as a time-space diagram.

Figure (a) shows that the speed of the VSL #21 continuously decreases. The speed contour map describes the low speed of the vehicles. To overcome this unrealistic behavior, we allowed for vehicles to accelerate when passing the bottlenecks, in accordance to current real-world operations, where drivers do not comply strictly with the posted VSL signs. Using this configuration of the model, we ran the optimization routines in GTSIM (as explained in chapter 4) to find the optimal parameters, and in the best case we found that travel times increase by approximately 7% compared to the situation of no control. This result is not surprising and accords well with experiences reported in the literature where the benefits of speed harmonization come from accident reductions rather than increases in freeway capacity.

This result prompted us to design a strategy to increase freeway capacity, as explained next.

3.2. Combined Variable Speed Limit-Ramp Metering Algorithm at Merge Bottleneck

The previous section has demonstrated that GDOT's current speed harmonization system on I-285 increases travel times by about 7% compared to no control. This is not surprising: existing implementations of VSL throughout the world, which are based on speed harmonization, have shown benefits stemming from incident reductions, but there is no evidence of freeway capacity improvements. Here we propose a new VLS strategy designed to increase capacity at metered on-ramp bottlenecks and show that it can reduce travel times by 8% in the corridor.

3.2.1. Problem Formulation

Consider an isolated merge bottleneck as illustrated in Figure 17, with λ_0 and λ_1 , representing the demands of the mainline and the on-ramp, respectively, and μ_2 , representing the capacity of the bottleneck, located in the merge area. Because of the capacity drop phenomenon, when queues form, the bottleneck capacity drops from μ_C to μ_2 (see Figure 18). According to Newell-Daganzo's merge model (Daganzo, 1995, 1996), traffic transitions at the merge depend on supply (μ_2, μ_C) and demand (λ_0, λ_1) (Figure 19). Our model assumes that total demand ($\lambda_0 + \lambda_1$) exceeds bottleneck capacity μ_2 so that current traffic is located in areas A_2, A_3 , and A_4 in Figure 19. In these areas, only flows q_0 and q_1 can enter the bottleneck, and queues form if these amounts exceed $(\lambda_0 - q_0, \lambda_1 - q_1)$.

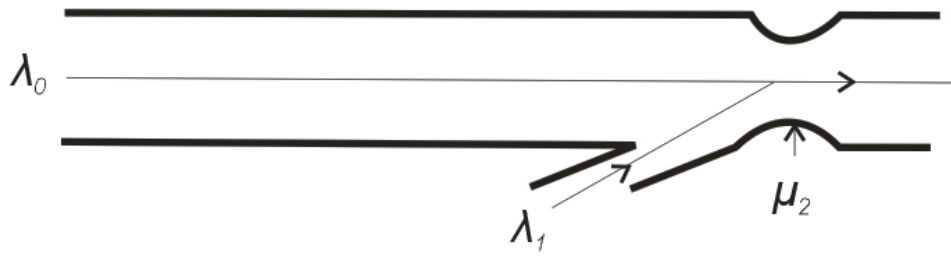


Figure 17 Isolated bottleneck at a merge area

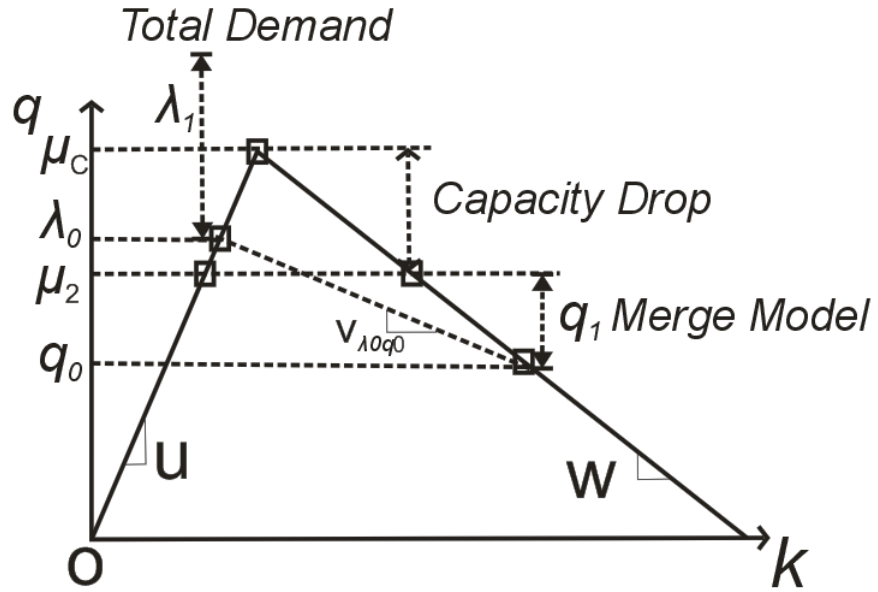


Figure 18 Capacity drop at a merge area. u : free-flow speed (km/hr), w : wave speed (km/hr), v : shock wave speed (km/hr), q : flow (vehicles/hr), k : vehicle density (veh/km)

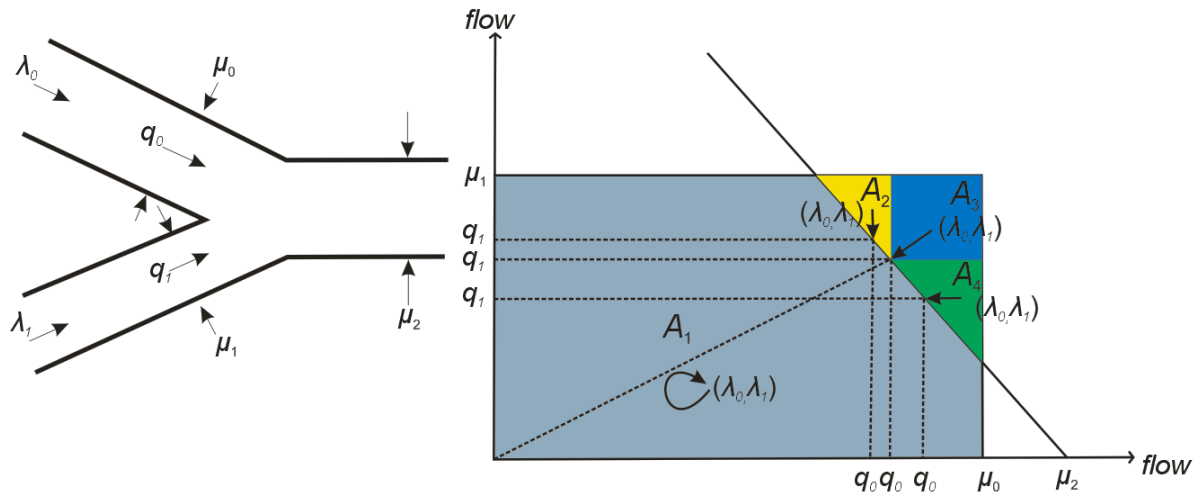


Figure 19 Newell-Daganzo merge model

3.3. Model

This section presents a VSL and ramp-metering strategy that controls traffic upstream of the merge area so that the traffic status switches from areas A_2, A_3, A_4 to area A_1 , shown in Figure 19, and results in increasing the bottleneck capacity of μ_2 to μ_c .

3.3.1. Preventing capacity drop using VSL

The VSL section, located upstream of the merge bottleneck (see Figure 20), is composed of two zones: a speed limit zone and an acceleration zone. The vehicles follow the posted speed limit when they travel within the speed limit zone and accelerate to free-flow after they pass the acceleration zone. Without ramp metering control, one scenario that could prevent capacity drop is to assign priority to the on-ramp flow, thereby preventing a queue from forming in the on-ramp (see Figure 21). The figure presents an

initial traffic condition A_1 of a merge model showing that the initial total demand is less than the freeway capacity, and a queue has not yet formed and a capacity drop has not occurred. After some time, suppose that the on-ramp flow demand increases and that the total demand exceeds the freeway capacity. At this point, we activate the VSL zone, with l_1 representing the length of the VSL zone and l_2 the length of the acceleration zone.

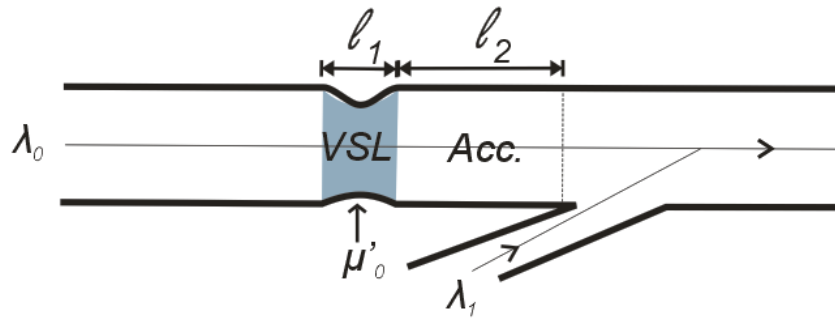


Figure 20 VSL upstream of the merge area

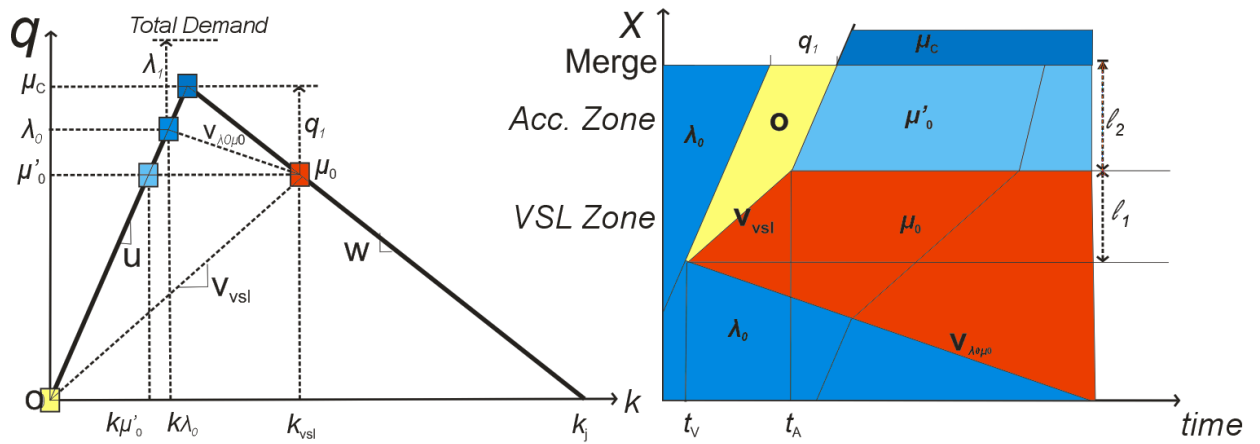


Figure 21 Fundamental mainline diagram and the time-space diagram representation of a strategy for eliminating on-ramp queue

As illustrated in the fundamental diagram in Figure 21, the speed in the limit zone, v_{vsl} , is given by

$$\mu_c - q_1 = w(k_j - k_{vsl}) = v_{vsl}k_{vsl}. \quad (1)$$

where μ_c is the maximum flow without a breakdown and $q_1 (= \lambda_1)$ is the on-ramp flow. Note that μ_c , w , and k_j are constants, and k_{vsl} is determined by the selection of q_1 .

Let t_v and t_A represent times when the first VSL-applied vehicle enters the VSL zone and the acceleration zone, respectively. At time t_v the flow in the VSL zone becomes μ_0 , and the density of the VSL zone becomes k_{vsl} . After t_A , the flow of the acceleration zone becomes μ'_0 because VSL-applied vehicles do not begin to accelerate after the lead vehicle accelerates, but instead, they exit the VSL zone and enter the acceleration zone. Assuming that vehicles accelerate to a free-flow speed quickly, the density of the acceleration zone decreases from k_{λ_0} to $k_{\mu'_0}$. This decrease creates more space for lane changing for the on-ramp flow, reducing the probability of a capacity drop.

We found two possible by-products of this system. When VSL is activated, the state of the traffic downstream of the first VSL-applied vehicle becomes the void state (O in the figure). Although this void induces a loss of capacity for a moment, it is useful, a topic that will be discussed in the next section. The potential drawback is that the queue forms upstream of the VSL zone in state μ_0 with shock speed $V_{\lambda_0\mu_0}$. We will show that as long as this shock does not reach the upstream ramp, benefits can be expected. To clarify this point, we illustrate the cumulative counts of vehicles at the beginning and end of the network in Figure 22. Solid lines represent the demand for each route, dashed lines depict the capacity drop situation (without VSL), and dotted lines show the application of the

VSL system. When VSL is applied, the slopes of the departure rate become steeper than they do when it is not applied, so the total travel time decreases.

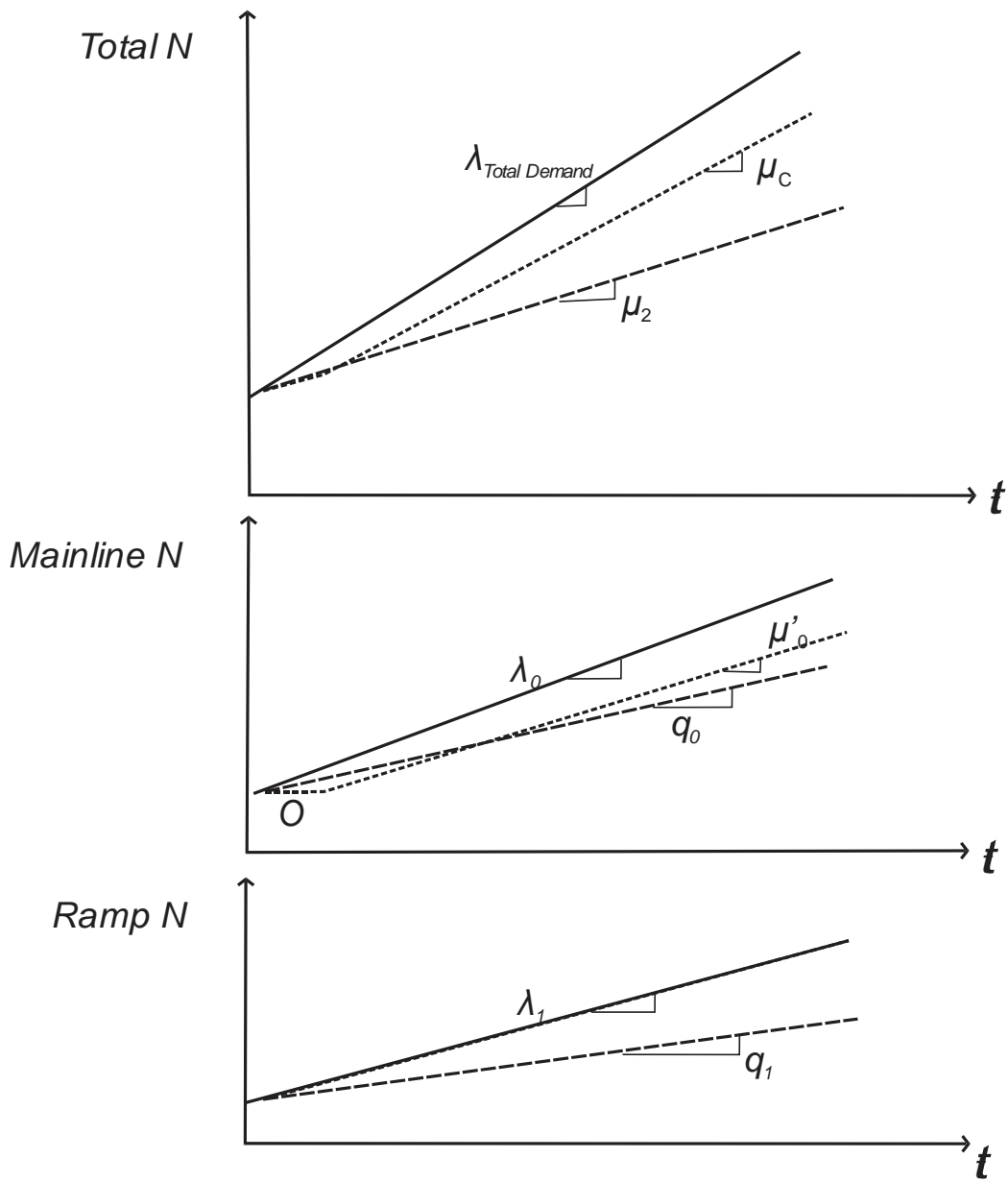


Figure 22 Cumulative count curves of the capacity drop and VSL. N: cumulative count of vehicles, t: time

3.3.2. Combined VSL and RM Model

In the previous section, we presented a VSL model that assigns priority to on-ramp traffic flow. However, this model may deteriorate mainline flow when on-ramp flow is abnormally high. To compensate for this problem, we propose a method combining ramp metering and that provides more flexibility in operation than the previous VSL system alone. Let us assume that $q_{1' RM}$ is the ramp metered rate; we then calculate the speed of the VSL and other corresponding traffic parameters from the following equation, which is similar to equation (1); that is,

$$\mu_c - q_{1' RM} = w(k_j - k_{vsl}) = v_{vsl}k_{vsl}. \quad (2)$$

The ramp-metering flow can be determined by the following methods:

Method 1: This method enhances mainline safety by maintaining speed v_{vsl} only slightly less than the previous mainline travel speed. This method predetermines v_{vsl} (e.g., $v_{vsl} = v_{free-flow} - 10_{mph}$) and then calculates ramp flow $q_{1' RM}$.

Method 2: This method uses the RM algorithm ALINEA (M. Papageorgiou et al., 1997; Markos Papageorgiou, Hadj-Salem, & Blosseville, 1990) (see Chapter 2):

$$r(t) = r(t - \Delta t) + K_R(\hat{o} - o_{out}(t)), \quad (3)$$

where $r(t)$ and $r(t - \Delta t)$ are the metering flow rates of the current and previous time steps (Δt is the length of the time period of updates), respectively, $o_{out}(t)$ is the occupancy of the current time step, and K_R is the constant defined by the operator.

In addition to enhancing flexibility and safety, the combined RM and VSL method fills the void (O) upstream of the first VSL-applied vehicle, explained in the

previous section, by controlling on-ramp flow. If we assume a given low metering rate and the formation of a queue behind the ramp signal, then both period (T) and maximum length (L) of void O are given by

$$T = l_1 \left(\frac{1}{v_{vsl}} - \frac{1}{v_f} \right) \quad (4)$$

$$L = \begin{cases} l_2, & v_f \cdot T = l_2 \\ v_f \cdot T, & v_f \cdot T < l_2 \\ l_2 + (l_1 - v_{vsl}) \cdot (l_1 + l_2) / v_f, & v_f \cdot T > l_2 \end{cases} \quad (5)$$

The number of free-flow accelerated vehicles from the queue at the on-ramp that can fill void O is $Q(t_{b'} - t_{a'})$, where Q is the capacity of the lane, $t_{b'}$ is the time that the first VSL-applied vehicle passes the merge line, and $t_{a'}$ is derived by $\frac{w}{w+v_{free-flow}} t_{b'}$, where the time that the last free-flow vehicle passes the merge is zero without loss of generality; see Figure 23.

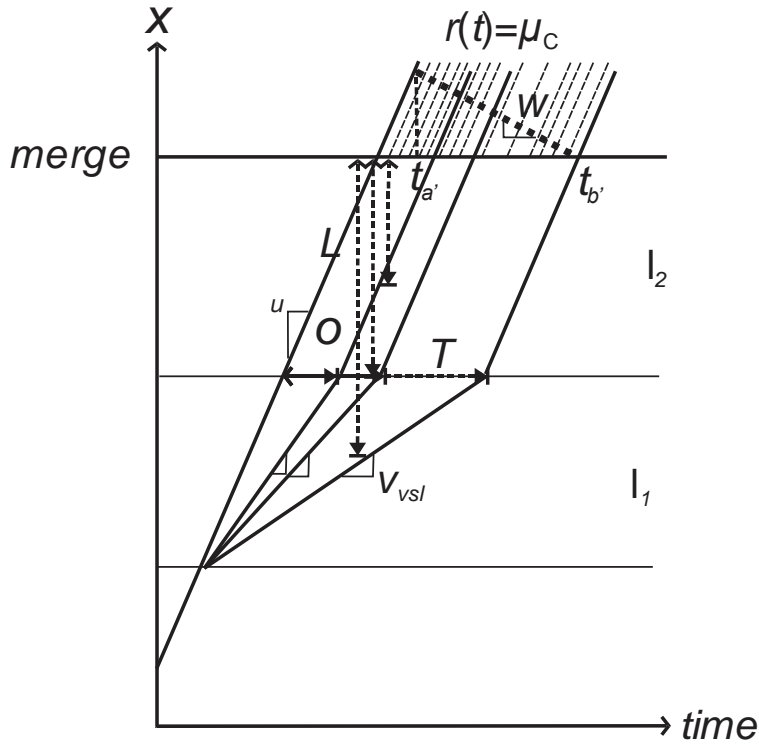


Figure 23 Time-space diagram of the metering rate during the void period

Method 3: This method, which uses the maximum metering rate of the ramp, $r(t)$ during period T , can be expressed as

$$r(t) = \mu_c, \quad (6)$$

We extend our problem to the recovery of the capacity drop. Assume that abrupt high demand of on-ramp traffic induces a capacity drop, illustrated in Figure 18. To resolve the capacity drop, an RM system restricts on-ramp flow up to the lowest metering rate, which is sufficient not to interrupt mainline flow at time t_{min_R} . As the mainline flow is protected from the on-ramp flow, the capacity is recovered to μ_c (Cassidy & Rudjanakanoknad, 2005), and the queue in the mainline diminishes and clears. When the

mainline queue clears, we activate the VSL at time $t_{VSL_{On}}$, as in Figure 21, to prevent the recurrence of the capacity drop. Also, using Method 3, we impose the metering rate of the ramp during the void period, $(t) = \mu_c$, which flushes the on-ramp queue. Figure 24 illustrates a time-space diagram of the integrated system. The figure shows that the entrance of the VSL zone meets the back of the queue at time VSL activation $t_{VSL_{On}}$. With current technology, the VSL zone, or speed limit signs, are prefixed, and VSL activation time $t_{VSL_{On}}$ is determined from RM activation time t_{min_R} .

The corresponding cumulative count curves of Figure 24 are illustrated in Figure 25. The solid and dashed lines are similar to those in Figure 22; dash-dotted lines depict the combined RM and VSL strategy. As expected, while the mainline flow rate increases after the ramp flow is metered, the ramp flow rate decreases until the queue clears and initiates the VSL. However, the total flow rate increases significantly so that the total travel time decreases. The following section presents a simulation approach that verifies the proposed strategy.

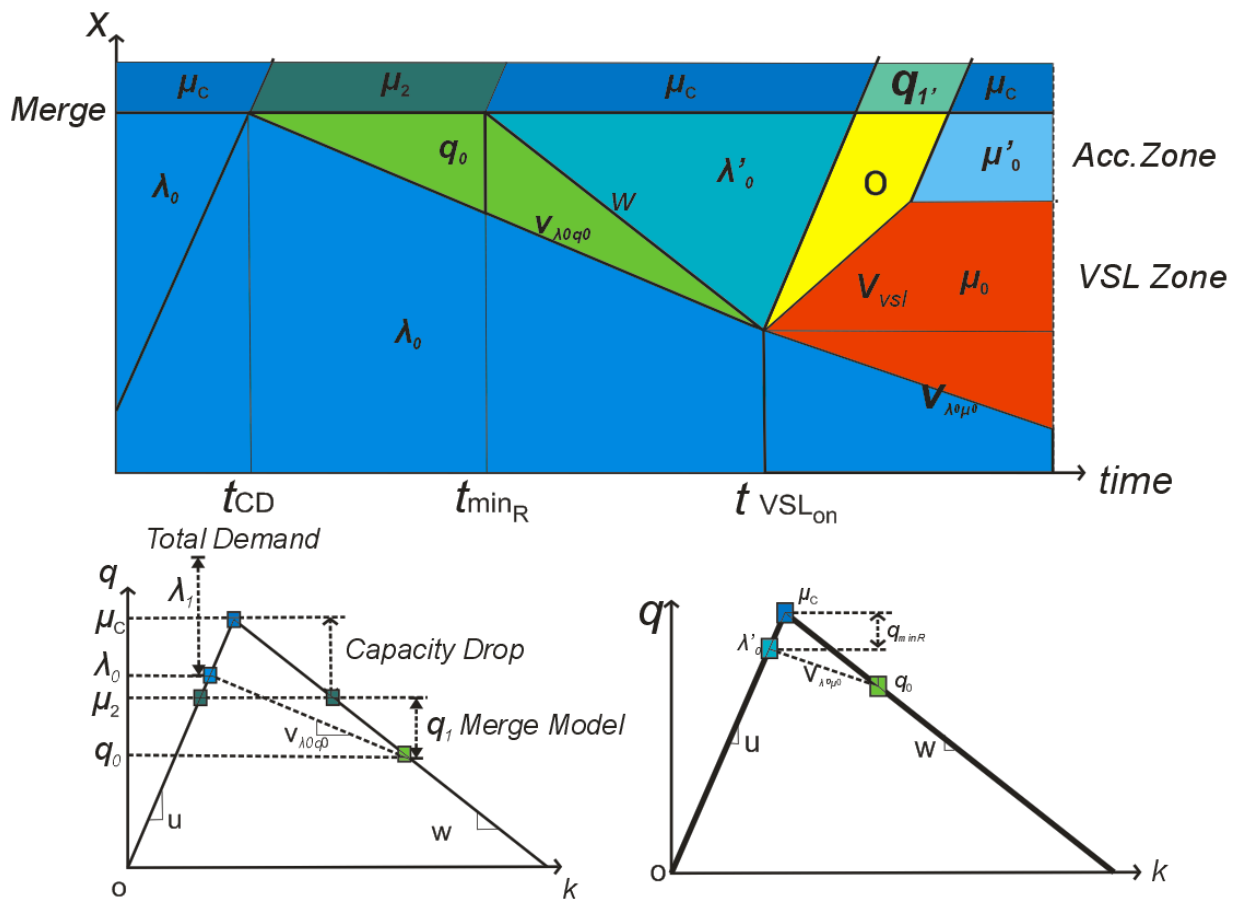


Figure 24 Time-space diagram of the recovery of the capacity drop using the integrated RM and VSL model for mainline traffic

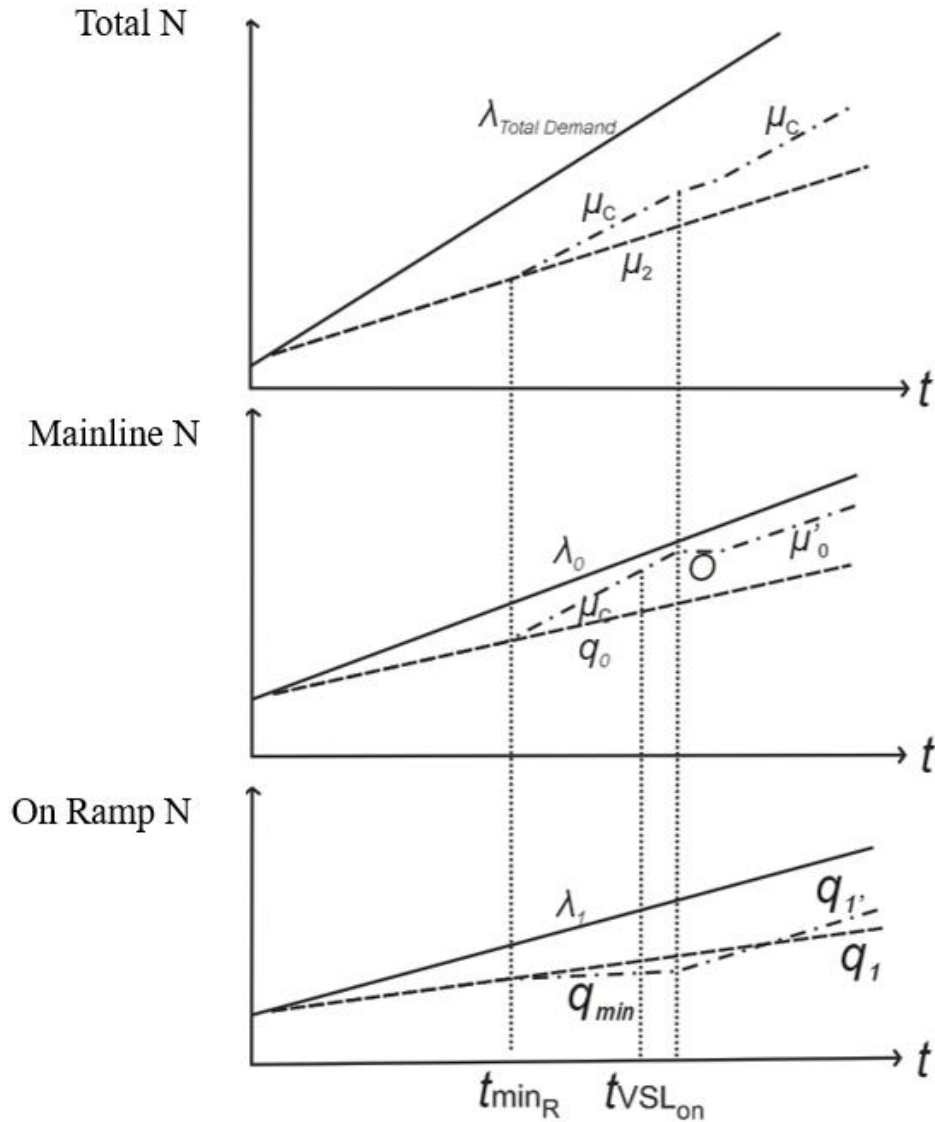


Figure 25 Cumulative count curve of Figure 23 and Figure 24. N: cumulative count of vehicles, t: time. The slope of the line means the flow at that time.

Method 4: This method always uses only the ramp metering system and activates the VSL only when the queue flush system becomes activated. It incorporates equation (2) into modified method 3.

In most cases, the ramp metering system is accompanied by a queue flush system that prevents the queue from spilling back to an arterial road. When the queue flush is activated, a ramp-metering signal is turned off, and the flow rate of ramp $r(t)$ becomes μ_c , as in method 3. However, although in the queue flush situation, we can control the ramp flow within the range of the demand of ramp $\lambda_1(t)$ and capacity μ_c ,

$$\lambda_1(t) \leq r(t) \leq \mu_c.$$

The speed of the VSL follows $\mu_c - r(t) = w(k_j - k_{vsl}) = v_{vsl}k_{vsl}$.

This page is intentionally left blank.

4. Optimization Framework

One of the most widely used stochastic simulation-optimization techniques in both engineering and social sciences is the genetic algorithm (GA). The evolution of the GA is successful, its method is robust to adapting to biological systems, and its parallel implementation with computer software and hardware is relatively easy. The GA searches for an optimal solution while iteratively evolving with the probabilistic selection, crossover, and mutation (Mitchell, 1997).

Two main components of this framework are the GA-based optimizer and GTsim module. The optimizer will provide a set of parameter values that are utilized by the GTsim module to estimate the total travel time that will be sent back to the optimizer. The GTsim application will provide continuous state information to the ramp metering algorithm that calculates metering rates based on the state information and the parameters provided by the GA based optimizer. The sections below describe GTsim and GA based optimizer as implemented in this study.

4.1. *GTsim Application*

GTsim, which is built based on a kinematic wave model, is the first one of its kind proven to replicate traffic dynamics during congestion. *GTsim* implements the latest lane-changing models, which significantly improved understanding of traffic congestion. Specific explanations on GTsim modules were introduced in the final report of the “Development of Optimal Ramp Metering Strategies” study (Guin & Laval, 2013).

4.2. Genetic Algorithm

The objective of this project is to find optimal combination of parameters of ramp metering for the study corridor. As the solution space is large, simulation-based optimization, genetic algorithm play an important role in converging to the global optimum. Parameters of the genetic algorithm were described in the final report of the “Development of Optimal Ramp Metering Strategies” study (Guin & Laval, 2013).

The study corridor has the following seventeen entry locations (referred to as “origins” for the OD terminology) that feed traffic to the network:

- Upstream Freeway, Peachtree Dunwoody Road, Ashford Dunwoody Road, North Peachtree Road, Peachtree Industrial Parkway, Buford Highway, the I-85 Connector, Chamblee Tucker Road, Lavista Road, Lawrenceville Highway, WB Stone Mountain Freeway (left lane merge), EB Stone Mountain Freeway, Church Street, Memorial Drive, Indian Creek Station Connector, Covington Highway, Glenwood Road.

The corridor has the following seventeen exit locations (referred to as “destinations”):

- Ashford Dunwoody Road, Chamblee Dunwoody Road, SB Peachtree Industrial Parkway, NB Peachtree Industrial Parkway, Buford Highway, the SB I-85 Connector, the NB I-85 Connector, Northlake Parkway, Lavista Road, Lawrenceville Highway, WB Stone Mountain Freeway, EB Stone Mountain Freeway, East Ponce de Leon Avenue, Memorial Drive, Covington Highway, Glenwood Road, Downstream Freeway.

5.2. Traffic Data Analysis

5.2.1. Data

Within the 19.25-mile study corridor, this study used 52 GDOT NaviGator's Vehicle Detection System (VDS) (Figure 27, Figure 28) data that collected 20-second interval volume, speed, and occupancy (hereafter referred to as the "VDS data"). This study extracted the 52-stations VDS data during a one-month period (April 2016).

All on- and off- ramps in the corridor except for six locations (the NB GA-400 on-ramp, the SB Peachtree Industrial Blvd off-ramp, the Buford Hwy on-ramp, the I-85 connector on-ramp, the WB Stone Mountain Fwy connector on-ramp, I-20 off-ramp) were inspected and five-minute volume data for 48 hours at these ramps were measured using traffic tube counts (see Figure 29, GDOT traffic tube counts for specific locations).

As traffic volume data are the main input variables of this simulation case study and containing the volume data for all ramps is critical, this study focused on identifying the five-minute traffic volume of the missing locations for the same 48 hours by analyzing VDS data and the upstream and downstream ramps of the missing locations. For example, for the SB Peachtree Industrial Blvd off-ramp, we compared the VDS data of detector ID 2850034, 2850036, 2850037, which are the NB Peachtree Industrial Blvd off-ramp, and the Peachtree Industrial Blvd on-ramp, respectively. We assumed that the mainline volume on the corridor would be conserved by adding or subtracting the ramp volume. However, a comparison of tube count data and the VDS data resulted in unreasonable ramp volumes (negative values) for the missing ramps.

The unrealistic ramp volumes could have resulted from the low-quality VDS data. For example, some detectors lost the data of one lane out of five or six lanes. We also tried to compensate for these missing lanes by multiplying the ratio of the missing lanes. However, we needed the lane distributions for each location to obtain the volume of correct whole lanes, which is beyond the scope of this study.

Because of these limitations, this study excluded the most upstream and downstream missing ramps, the GA-400 on-ramp, and the I-20 off-ramp. This exclusion, however, did not affect the system corridor because the GA-400 on-ramp does not contain a ramp-metering system, and the I-20 off-ramp does not affect congestion in the corridor.

Inventory | 🌐 📄 🖨️ 🗑️

VDS ID# **GDOT-STN-2850023** AGENCY: **GDOT** [View Only](#)

Device Information

ID: **GDOT-STN-2850023**

Active: **Y**

Device ID: **2850023**

VDS Type: **microwave_radar**

Location Information

Roadway Type: **Interstate**

Roadway Name: **I-285 (Northern)**

Direction: **E**

Cross Street: **PEACHTREE DUNWOODY RD**

City: **Atlanta**

District: **D7 Chamblee**

County:

Mile Marker: **27.74**

State: **GA**

Vendor Information

Vendor Name: **Traficon**

Protocol Name: **Traficon**

Detectors Information

Lane Number	Lane Type	Detector ID
1	through lanes	1
2	through lanes	2

Select a Device ▼

Geographical Information

Latitude: **33.91581**

Longitude: **-84.3425**

Leash Length: **0**

Angle: **0**

Orientation: **0**

Communication Information

Comm Type: **TCP**

Host/IP: **192.168.202.133**

Port: **5000**

Drop ID: **0**

Msg Type: **PMPP**

Community: **public**

Optionals: **proxy=TraficonVDS;cam=0; lane=1-2-3-4-5-6**

Administration Information

Description: **PEACHTREE DUNWOODY RD**

Date Created: **-**

Date Modified: **09/08/2014 - V0003468**

Modify Previous Next New

DMS
CCTV
VDS
TTPaths
Contacts
Gate
VSL
LCS
HERO
Signals

Figure 27 GDOT NaviGator video detection system (VDS)

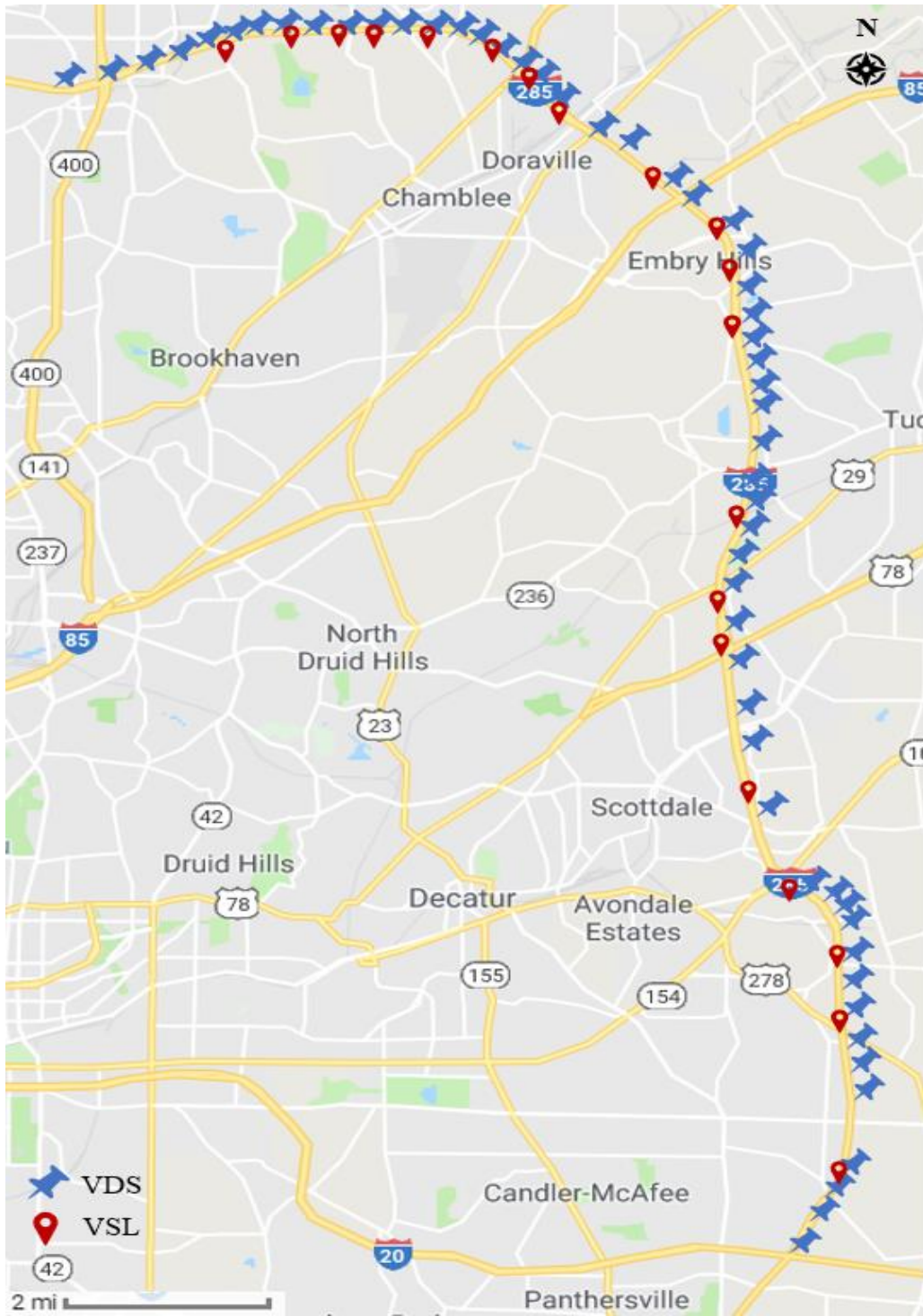


Figure 28 Locations of GODT NaviGator’s Vehicle Detection System (blue) and Variable speed limit (red) on Google Map.

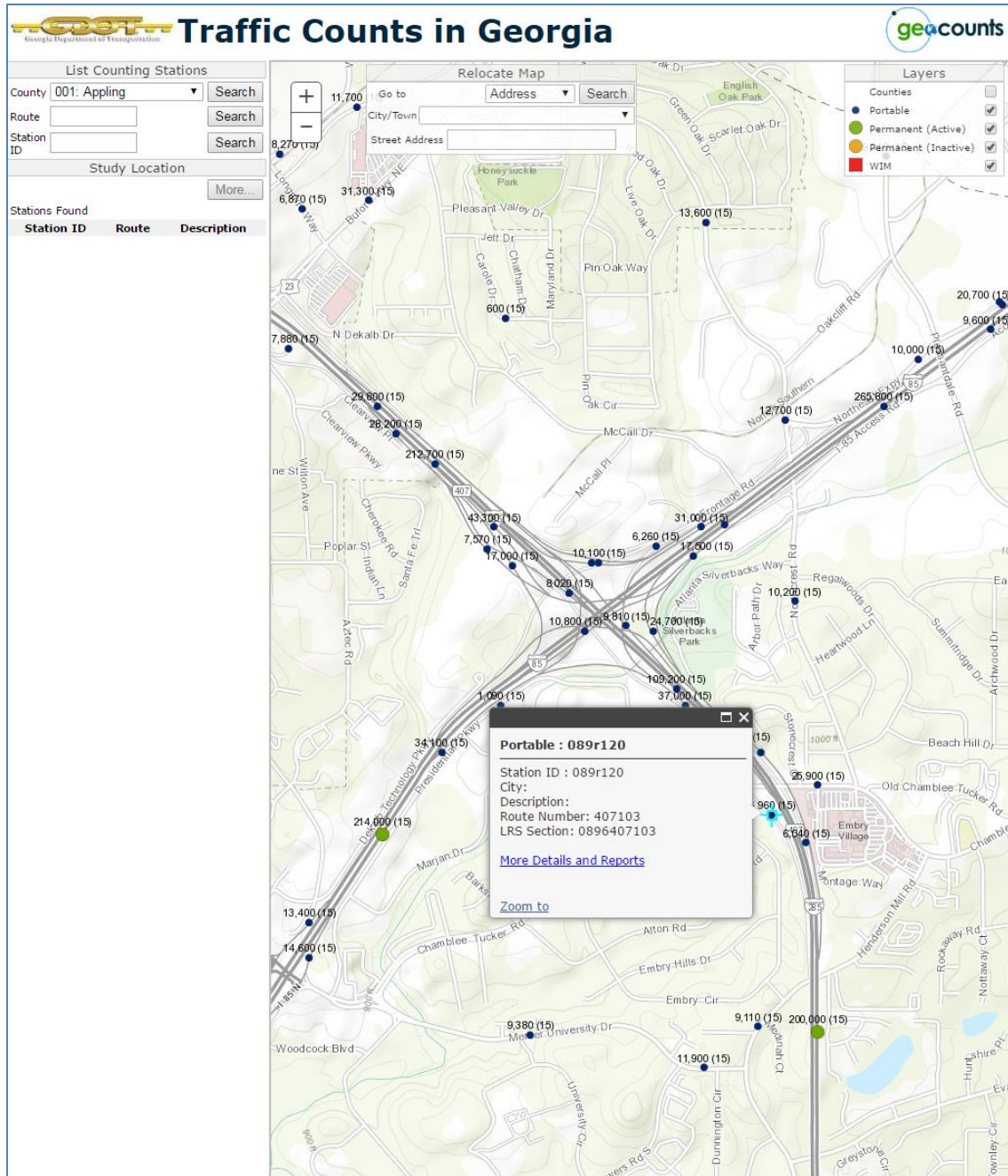


Figure 29 GDOT traffic tube counts

5.2.2. Data Processing for Origin Destination Matrix Estimation

Rationally estimated origin-destination traffic volume matrix is essential in this simulation-based research. Figure 30 describes the steps of the O/D matrix estimation. We first extracted the traffic volume of the on-ramp (origin) and the off-ramp (destination) for the time periods of interest (PM peak) from the tube counts and the VDS volume data. We also calculated the travel time across each origin and destination using the space-mean speed that was converted from VDS speed data.

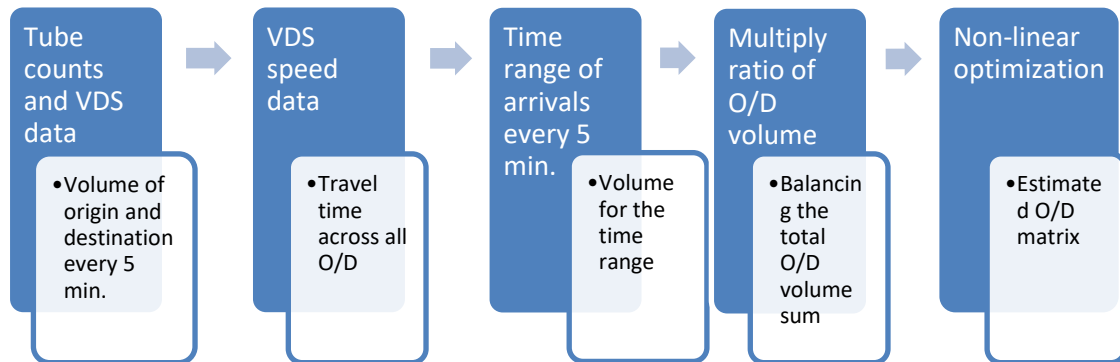


Figure 30 Flow chart of O/D matrix estimation

Using these travel time data, we produced the possible time range of the arrival of the origin traffic. For example, for the I-285 downstream freeway destination, the earliest time of arrival would be the time that the first vehicle departed from the closest origin, Glenwood Road, and arrived at the destination from the beginning of the time period. Similarly, the latest time of arrival would be the time that the last vehicle departed from the farthest origin, I-285 Upstream freeway, and arrived at the destination from the end of the time periods. Using these possible time ranges of arrival, we calculated the arrival traffic volume for each destination.

The target time periods of our research are before the onset of the off-peak. From the typical traffic data of Google Maps, we found that off-peak congestion on our research corridor formed before 3:00 PM. Therefore, we chose 2:30 PM to 3:30 PM (60 minutes) as the time periods for this study.

The time periods of the origin traffic were set at 60 minutes. However, the calculated possible time periods of destination traffic were longer than 60 minutes as they were affected by congestion. To meet the total sum of the origin and destination traffic, we adjusted the destination traffic volume by multiplying the ratio of the sum of the origin volume to the sum of the possible destination volume.

After matching the sum of the origin and destination traffic volume, we estimated the O/D matrix using a nonlinear optimization method. We explain the assumptions and constraints of this optimization method using the simple network below (Figure 31).

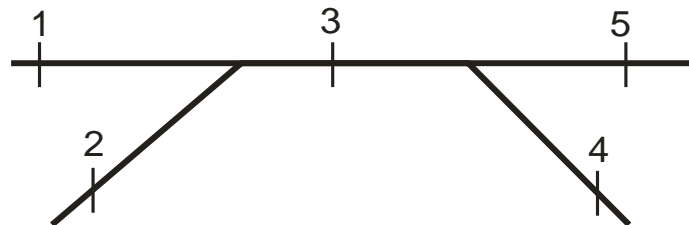


Figure 31 Sample network for OD estimation

This network consists of two origins (1, 2) and two destinations (4,5). From observed data (i.e., tube counts, VDS), the volumes of each origin and destination are generated (1-A, 2-B, 4-C, and 5-D). The volume of section 3 is calculated by adding the volumes of sections 1(A) and 2(B). To calculate the destination specific volumes, we generated the O/D matrix as Table 2. Constraints are that the sum of each row and

column volumes are close to the total estimated volume. For example, a volume that is generated from section 1(a) is composed of volumes heading to 4 (α) and 5(β). In this case, we set constraint $\alpha + \beta \leq a$. Other rows and columns work in a similar manner. Subsequently, we generated a volume-calculation table, Table 3, and then we can calculate the O/D matrix using the optimization function. In the mathematical formulation, the objective function and constraints are described as follows.

$$obj.: \min. (A - a)^2 + (B - b)^2 + (A + B - a - b)^2 + (C - c)^2 + (D - d)^2$$

$$\text{Subject to } \alpha + \beta \leq a, \gamma + \delta \leq b, \alpha + \gamma \leq c, \beta + \delta \leq d$$

Table 2 Sample O/D calculation table

O \ D	4	5	TARGET	SUM
1	α	β	A	a
2	γ	δ	B	b
TARGET	C	D		
SUM	c	d		

Table 3 Sample calculated and observed flow

	Calculated	Observed	Square of Differences
1	a	A	$(A - a)^2$
2	b	B	$(B - b)^2$
3	a+b	A+B	$(A + B - a - b)^2$
4	c	C	$(C - c)^2$
5	d	D	$(D - d)^2$

We used the computer program Generalized Reduced Gradient Algorithm (Lasdon, Fox, & Ratner, 1974), which is useful for solving the nonlinear optimization problem. The objective function of our problem is to minimize the total sum of the squared differences of the estimated volume (last column of Table 4), and the constraints are the sums of each cell of rows and columns (see Figure 32 O/D matrix). In Table 4, the green cells represent origin traffic, and the pink cells indicate destination traffic. In Figure 32, the gray cells must be zero because these destinations are upstream of the origins. With the algorithm, we found that the objective value decreased to a two-digit value.

Table 4 Flow calculation

Link	Ramps	Calculated Flow	Observed Flow	Difference	Difl. sqrd.
1	U/S Fwy	7914	7914	0	0
2	Peachtree Dunwoody	1030	1030	0	0
3		8944	8944	0	0
4	Ashford Dunwoody	1317	1317	0	0
5		7627	7627	0	0
6	Ashford Dunwoody	1279	1279	0	0
7		8906	8906	0	0
8	Chamblee Dunwoody	1099	1099	0	0
9		7807	7807	0	0
10	North Peachtree	978	978	0	0
11		8785	8785	0	0
12	SB P'tree Ind.	189	189	0	0
13		8596	8596	0	0
14	NB P'tree Ind.	1492	1492	0	0
15		7104	7104	0	0
16	P'tree Ind.	1963	1963	0	0
17		9067	9067	0	0
18	Buford Hwy	577	577	0	0
19		8490	8490	0	0
20	SB I-85	1440	1440	0	0
21		7050	7050	0	0
22	NB I-85	3181	3181	0	0
23		3869	3869	0	0
24	Buford Hwy	411	411	0	0
25		4280	4280	0	0
26	I-85	3941	3941	0	0
27		8221	8221	0	0
28	Chamblee Tucker	428	428	0	0
29		8649	8649	0	0
30	Northlake Pkwy	1055	1055	0	0
31		7594	7594	0	0
32	Lavista	996	996	0	0
33		6598	6598	0	0
34	Lavista	1063	1063	0	0
35		7661	7661	0	0
36	Lawrenceville Hwy	647	647	0	0
37		7014	7014	0	0
38	Lawrenceville Hwy	502	502	0	0
39		7516	7516	0	0
40	Stone Mt.	910	910	0	0
41		6606	6606	0	0
42	Stone Mt. EB	1276	1276	0	0
43		5330	5330	0	0
44	Stone Mt. Left merge	1017	1017	0	0
45		6347	6347	0	0
46	Stone Mt.	587	587	0	0
47		6934	6934	0	0
48	E Ponce De Leon	664	664	0	0
49		6270	6270	0	0
50	Church St.	382	382	0	0
51		6652	6652	0	0
52	Memorial Dr.	1008	1008	0	0
53		5644	5644	0	0
54	Memorial Dr.	891	891	0	0
55		6535	6535	0	0
56	Indian Creek	21	22	1	1
57		6556	6557	1	0
58	Covington	666	666	0	0
59		5891	5891	0	0
60	Covington	593	593	0	0
61		6484	6484	0	0
62	Glenwood	484	484	0	0
63		5999	6000	1	1
64	Glenwood	507	508	1	1
65		6506	6508	2	4
66	I-20	3203	3200	-3	9
67	D/S Fwy	3303	3300	-3	9

Origin/Destination		Ashford Dunwoody	Chamblee Dunwoody	SB P'tree Industrial	NB P'tree Industrial	Buford Hwy	SB I-85	NB I-85	Northlake pkwy	Lavista	LAWRENCE VILLE HWY	STONE MOUNTAIN FWY	STONE MOUNTAIN FWY EB	EAST PONCE DE LEON AVE	Memorial	Covington	Glenwood	I20	d/s Fwy	Target	Sum
		4	6	8	10	12	14	16	22	24	26	28	30	34	36	40	42	44	46		
u/s Fwy	1	1316	984	189	1258	1	1104	1196	114	99	533	130	120	232	121	0	0	298	219	7914	7914
P'tree Dunwoody	3	1	68	0	136	7	101	523	0	2	8	2	1	6	0	1	0	88	86	1030	1030
Ashford Dunwoody	5		47	0	67	36	98	786	0	1	4	0	26	3	0	1	0	109	99	1279	1279
N. P'tree Rd	7			0	30	22	72	654	0	1	4	0	25	3	0	2	1	85	79	978	978
P'tree Industrial	11					512	65	22	174	152	47	201	246	0	212	21	310	2	0	1963	1963
Buford Hwy	17								24	15	0	21	44	2	13	0	1	159	132	411	411
I-85 C/D SYS	19								722	714	12	464	615	295	386	11	0	270	453	3941	3941
CHAMBLEE TUCKER RD	21								22	12	2	9	43	1	14	0	0	160	165	428	428
Lavista Rd	25										36	57	103	36	73	8	2	365	381	1063	1063
Lawrenceville Hwy	27											24	52	0	23	0	0	222	180	502	502
Stone Mt. FWY Left	31													68	92	0	0	361	496	1017	1017
Stone Mt. FWY	33													18	41	10	67	199	252	587	587
Church St.	35														32	11	78	117	145	382	382
Memorial Dr.	37															601	1	140	149	891	891
Indian Creek	39															0	0	21	0	22	21
Covington	41																25	290	278	593	593
Glenwood	43																	319	188	508	508
	Target	1317	1099	189	1492	577	1440	3181	1055	996	647	910	1276	664	1008	666	484	3200	3300	8	
	Sum	1317	1099	189	1492	577	1440	3181	1055	996	647	910	1276	664	1008	666	484	3203	3303		0
		1317	1099	189	1492	577	1340	3081	955	896	547	810	1176	564	908	566	384	2929	3183		

Figure 32 O/D matrix

5.2.3. Calibration and Validation

GTsim has several parameters that must be calibrated (Bhargava Rama Chilukuri, Laval, & Guin, 2014). The parameters are categorized into capacity parameters (i.e., free-flow speed, jam density, and wave speed), lane-changing parameters (i.e., longitudinal distance between a vehicle and an exit ramp, tau (i.e., time to execute a lane-changing maneuver), epsilon (i.e., relaxation speed gap), and driver behavior parameters (friction speed). These calibrated parameters are summarized in Table 5. We used all parameter values in Table 5 for the entire corridor, except the value for the parameter of the longitudinal distance between a vehicle and an exit ramp. For some sections of the study corridor, the higher value of this parameter was needed to replicate feasible congestion propagation.

Table 5 Calibrated Parameters

Calibrated Parameter	Parameter Value
Free-flow speed	100 <i>km/hr</i>
Jam density	150 <i>veh/km</i>
Wave speed	20 <i>km/hr</i>
Longitudinal distance between a vehicle and an exit ramp	2 (4) <i>km</i>
Tau (time to execute a lane-changing maneuver)	4 <i>s</i>
Epsilon (relaxation speed gap)	2
Friction speed	20 <i>km/hr</i>

We validated the model by comparing the speed contour maps of (a) NaviGator's VDS data (2016/04/12) and (b) GTsim (see Figure 33), which used estimated the O/D flow of the same day data. In Figure 33, the color legend shows the speed scale (unit: *km/hr*). Note that in the speed plot of NaviGator (Figure 33 (a)), vehicle speeds over 100 (*km/hr*) are capped at 100 (*km/hr*) to meet the free-flow speed of GTsim. We found that in the real-world corridor on the date (Figure 33 (a)), congestion formed around the 34-mile post area at about 2:45 PM and around the 38-mile post area at about 3:30 PM. We confirmed similar patterns in the GTsim plots (Figure 33 (b)).

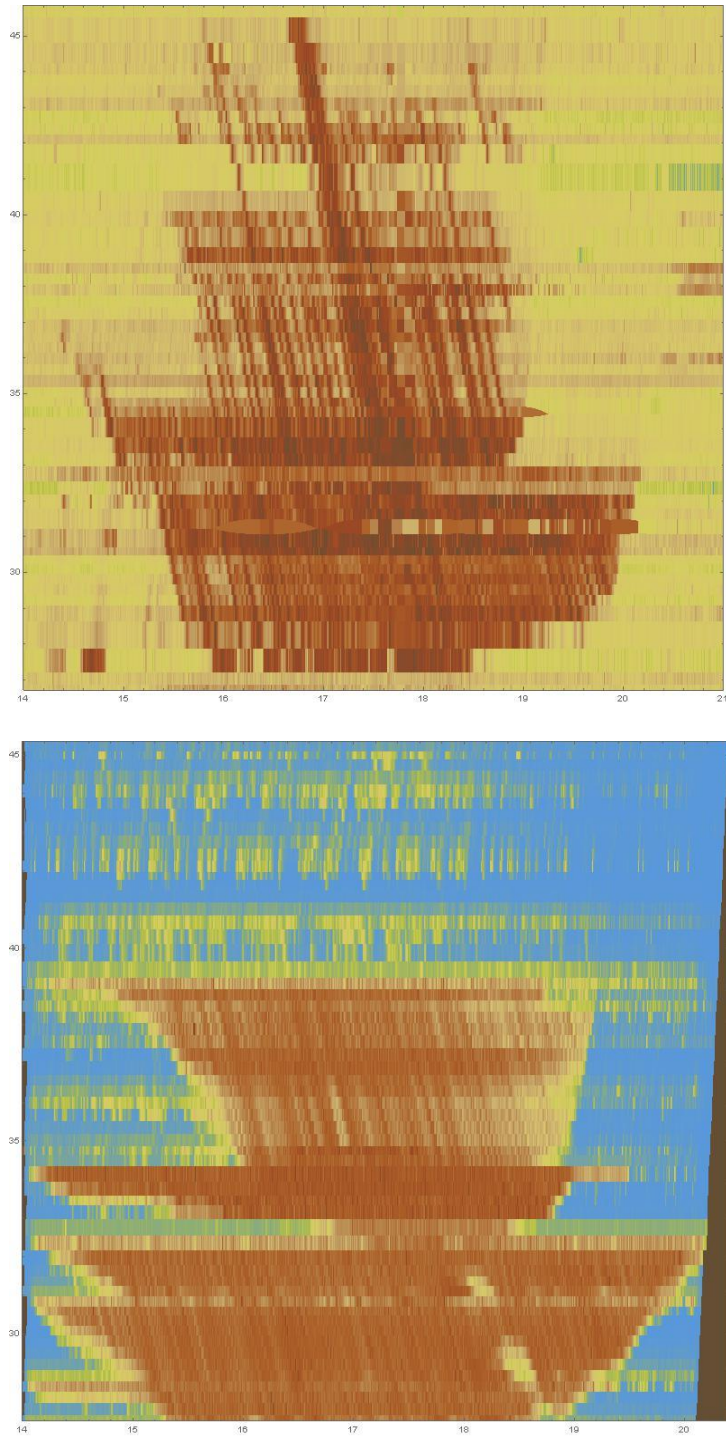


Figure 33 (a) Time Space Speed map of NaviGator (field data) (b) Time Space Speed map of GTsim (simulation)

6. Results

The results of the simulation-optimization for three cases (no control, the RM control only, the VSL-RM control) are summarized in Table 6. We found that the performance of the VSL-RM control with optimized parameters outperforms the RM control only model with its optimized parameters in terms of reducing total travel time. We also found that the current GDOT's VSL control worsens traffic in terms of travel time of the study corridor.

Table 6 Travel time (vehicle hours) comparison of no control, the RM control only, the VSL-RM control cases, and the current GDOT's VSL control

Case	System	Ramp	Freeway
No control	6561	175	6386
RM control only	6254 (4.7%)	194 (-10.9%)	6061 (5.1%)
VSL-RM control	6038 (8.0 %)	192 (-9.7%)	5846 (8.5%)
Current GDOT's VSL Control	6999 (-6.7%)	188 (-7.4%)	6811 (-6.7%)

Figure 34 to Figure 36 show the speed contour maps of each control case. In the figure, we found that most congestion arises upstream of the 32-milepost. The VSL in

this study corridor is located at the 34-milepost, and the target bottleneck location is downstream of the 35-milepost, highlighted by the red oval line in the figures. We found that both controls reduce congestion in the target area. The main benefits of the controls are that they delay the bottleneck formation time and lessen the severity of the bottleneck (passing speed).

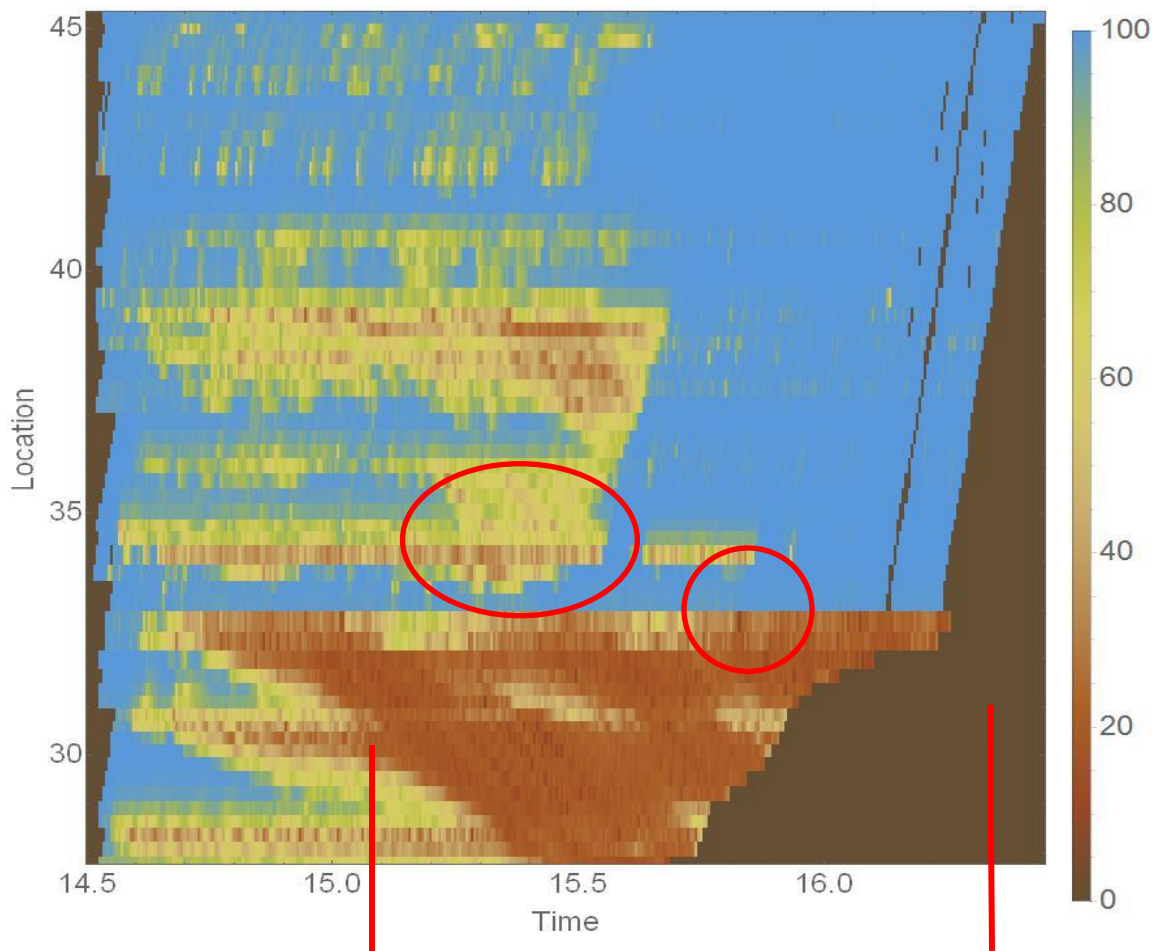


Figure 34 Speed contour map of the no control case. High speed areas are in blue and low speed areas are in brown. Red circles represent congestion areas to be compared with other figures. The legends are same for Figure 35 and Figure 36.

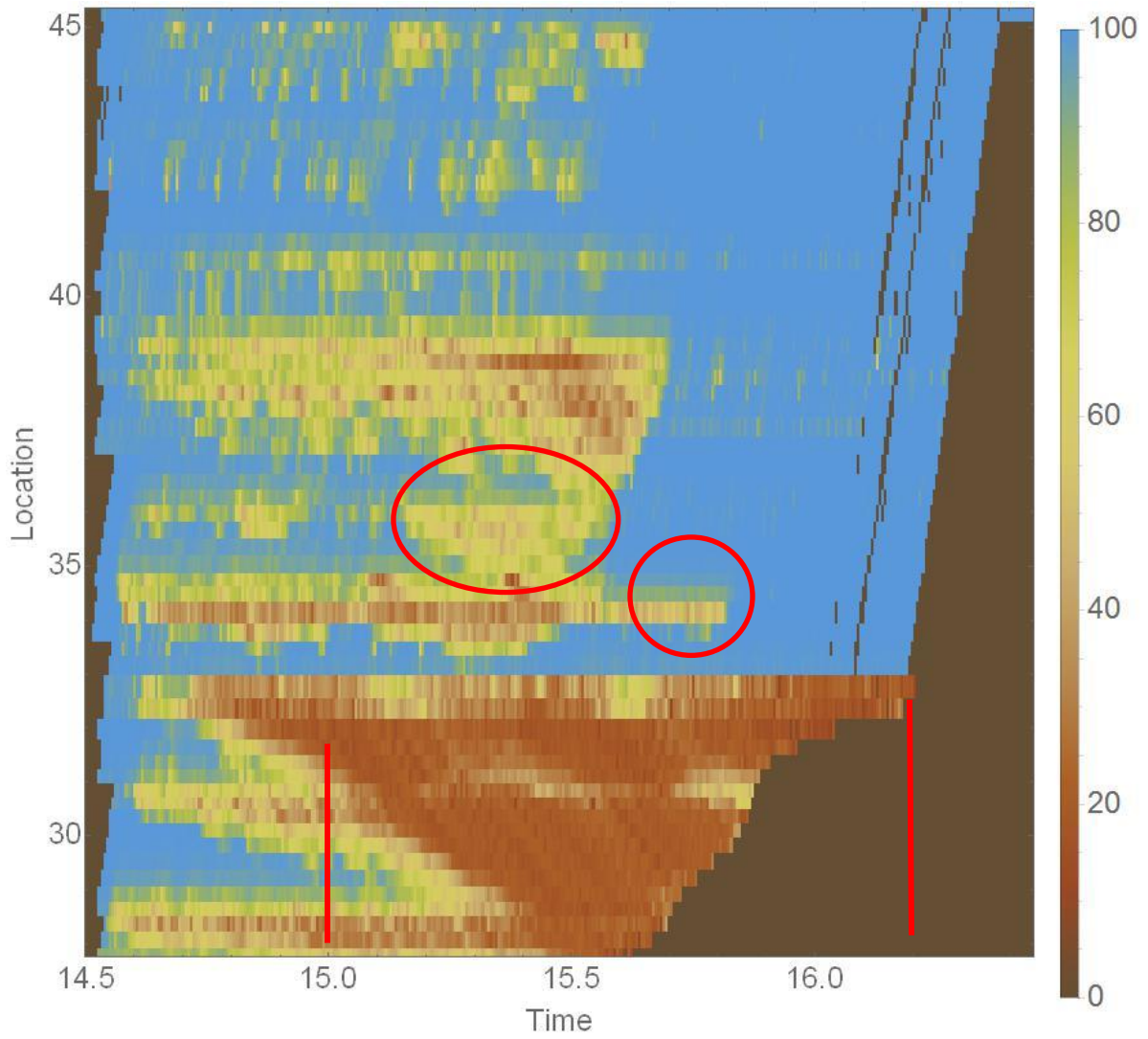


Figure 35 Speed contour map of the RM only control case. The results are slightly better than the no-control case based on the comparison of speed in the circled areas in Figure 34 and this figure.

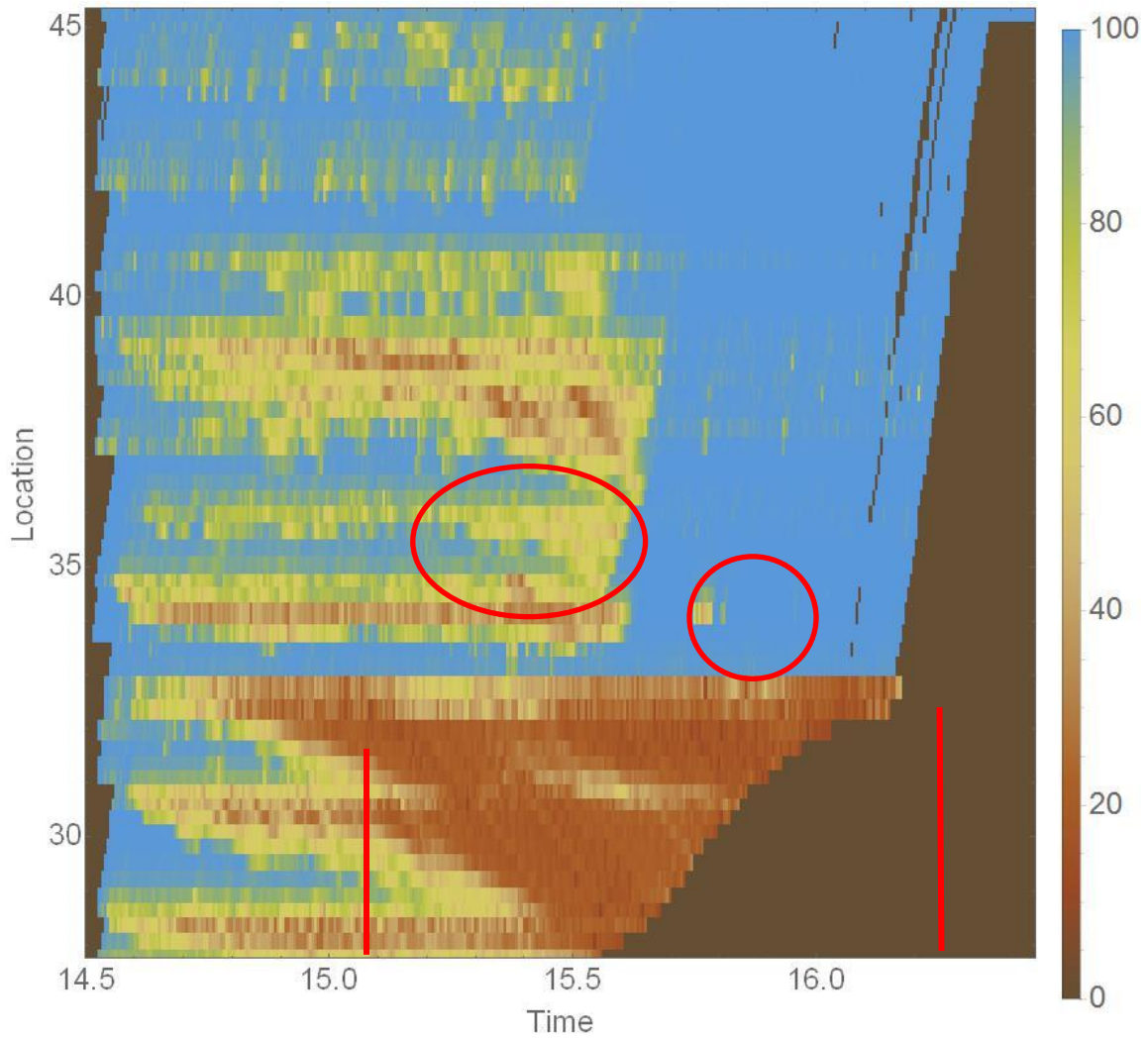


Figure 36 Speed contour map of the VSL-RM control case. The results are better than no-control case and the RM only case based on the higher speed shown in the red circles compared to Figure 34 and Figure 35.

All possible values for the K_R parameters and the solution spaces of the VSL parameters are very large. The genetic algorithm (GA) ran for up to 500 generations. After 300 generations, the GA converged to a minimum. To confirm that it was truly the global minima, tens of thousands of combinations of allowable values of impact parameters were also simulated. We found that the minimum obtained from the GA after 300 generations was indeed the global minimum. Thus, it was confirmed that the GA parameters used above will converge to the global minimum. This optimal parameter set, however, is very sensitive possibly because bottlenecks are correlated, not isolated. Table 7 summarizes the optimal parameter values of the RM only system and the VSL-RM system.

Table 7 Optimal parameter values of the RM only and VSL-RM models

Location	K_R	K_R (VSL+RM)
	(RM only)	
Ashford Dunwoody Rd	118	138
North Peachtree Rd	92	103
Peachtree Industrial Blvd	95	145
Chamblee Tucker Rd	151	84
Lavista Rd	120	114
Lawrenceville Hwy	106	132
Church St	124	111
Memorial Dr	106	122
Covington Hwy	142	79
Glenwood Rd	104	122

7. Conclusions

The objective of this study was to develop effective VSL control algorithms to minimize the total travel time on I-285 study corridor. However, since current GDOT's VSL algorithm-speed harmonization cannot improve traffic congestion in the simulation model, we proposed a combined VSL-RM model to prevent capacity drop at merge bottleneck. By determining optimal parameter values of the combined VSL-RM systems, this study presented the stochastic simulation-based optimization framework that integrates GTsim and the GA-based optimization module. With these optimal parameter values, we compared the minimum total travel time of the two systems to the no control case. We found that the optimal values derived from this case study, compared to the no-metering case scenario, reduce travel times by more than 8%. The optimal parameter values derived in this case study are temporal and location sensitive and need to be optimized for other locations and time periods. However, the optimization framework developed in this study can be seamlessly used to generate optimal parameters for other locations.

Regarding the implementation plan for the strategy proposed in this report, it has come to our attention that GDOT is about to deploy a new version of MaxView that will enable real-time control, which is a requirement of our proposed strategy. Unfortunately, the specifications of the new system were not available as of the writing of this report, and therefore an implementation plan cannot be included here. However, this implementation plan is the focus of a follow-up ongoing project.

This page is intentionally left blank.

8. References

- Abdel-Aty, M., Cunningham, R. J., Gayah, V. V., & Hsia, L. (2009). Dynamic Variable Speed Limit Strategies for Real-Time Crash Risk Reduction on Freeways. *Transportation Research Record: Journal of the Transportation Research Board*, 2078, 108–116. <https://doi.org/10.3141/2078-15>
- Abdel-Aty, M., Dilmore, J., & Dhindsa, A. (2006). Evaluation of variable speed limits for real-time freeway safety improvement. *Accident Analysis and Prevention*. <https://doi.org/10.1016/j.aap.2005.10.010>
- Abdel-Aty, M., Pande, A., Lee, C., Gayah, V., & Dos Santos, C. (2007). Crash risk assessment using intelligent transportation systems data and real-time intervention strategies to improve safety on freeways. *Journal of Intelligent Transportation Systems*, 11(3), 107–120.
- Allaby, P., Hellinga, B., & Bullock, M. (2007). Variable speed limits: Safety and operational impacts of a candidate control strategy for freeway applications. *IEEE Transactions on Intelligent Transportation Systems*, 8(4), 671–680. <https://doi.org/10.1109/TITS.2007.908562>
- Bertini, R., Boice, S., & Bogenberger, K. (2006). Dynamics of Variable Speed Limit System Surrounding Bottleneck on German Autobahn. *Transportation Research Record*, 1978, 149–159. <https://doi.org/10.3141/1978-20>
- Carlson, R. C., Papamichail, I., & Papageorgiou, M. (2011). Local feedback-based mainstream traffic flow control on motorways using variable speed limits. *IEEE*

Transactions on Intelligent Transportation Systems, 12(4), 1261–1276.
<https://doi.org/10.1109/TITS.2011.2156792>

Carlson, R. C., Papamichail, I., & Papageorgiou, M. (2014). Integrated feedback ramp metering and mainstream traffic flow control on motorways using variable speed limits. *Transportation Research Part C: Emerging Technologies*, 46, 209–221.
<https://doi.org/10.1016/j.trc.2014.05.017>

Carlson, R. C., Papamichail, I., Papageorgiou, M., & Messmer, A. (2010a). Optimal mainstream traffic flow control of large-scale motorway networks. *Transportation Research Part C: Emerging Technologies*, 18(2), 193–212.
<https://doi.org/10.1016/j.trc.2009.05.014>

Carlson, R. C., Papamichail, I., Papageorgiou, M., & Messmer, A. (2010b). Optimal Motorway Traffic Flow Control Involving Variable Speed Limits and Ramp Metering. *Transportation Science*, 44(2), 238–253.
<https://doi.org/10.1287/trsc.1090.0314>

Cassidy, M. J., & Rudjanakanoknad, J. (2005). Increasing capacity of an isolated merge by metering its on-ramp. *Transportation Research Part B*, 39(10), 896–913.

Chang, G.-L., Park, S. Y., & Paracha, J. (2011). Intelligent transportation system field demonstration: integration of variable speed limit control and travel time estimation for a recurrently congested highway. *Transportation Research Record*, 2243(2243), 55–66. <https://doi.org/10.3141/2243-07>

Chen, D., & Ahn, S. (2015). Variable speed limit control for severe non-recurrent

freeway bottlenecks. *Transportation Research Part C: Emerging Technologies*, 51, 210–230. <https://doi.org/10.1016/j.trc.2014.10.015>

Chen, D., Ahn, S., & Hegyi, A. (2014). Variable speed limit control for steady and oscillatory queues at fixed freeway bottlenecks. *Transportation Research Part B: Methodological*, 70, 340–358. <https://doi.org/10.1016/j.trb.2014.08.006>

Chilukuri, B. R. (2015). *Optimal Ramp Metering Of Freeway Corridors*. Georgia Institute of Technology.

Chilukuri, B. R., Laval, J. A., & Guin, A. (2014). MicroSimulation-Based Framework for Freeway Travel Time Forecasting. *Transportation Research Record: Journal of the Transportation Research Board*, 2470, 34–45.

Chilukuri, B. R., Laval, J. a, & Chen, D. (2013). Some Traffic Features During On-ramp Queue Flush. In *Transportation Research Board 92nd Annual Meeting* (pp. 1–15).

Daganzo, C. F. (1995). The cell transmission model. Part II: Network traffic. *Transportation Research Part B*, 29(2), 79–93.

Daganzo, C. F. (1996). The nature of freeway gridlock and how to prevent it. *Proceedings of 13th International Symposium on Transportation and Traffic Theory*, 629--646.

Duret, A. (2014). A multi-lane capacity model designed for variable speed limit applications. In *Transport Research Arena, Paris* (pp. 1–13).

Duret, A., Ahn, S., & Buisson, C. (2012). Lane flow distribution on a three-lane freeway: General features and the effects of traffic controls. *Transportation Research Part C*:

Emerging Technologies, 24, 157–167. <https://doi.org/10.1016/j.trc.2012.02.009>

Fang, J., Hadiuzzaman, M., Karim, A., Luo, Y., & Qiu, T. (2014). Variable Speed Limit Control Strategy with Collision Probability Assessments Based on Traffic State Prediction. *Transportation Research Record: Journal of the Transportation Research Board*, 2435, 11–18. <https://doi.org/10.3141/2435-02>

Guin, A., & Laval, J. (2013). *Development of Optimal Ramp Metering Strategies Final Report (GDOT Research Project TO 02-98; RSCH PROJ 11-18 Georgia Tech Project No. 2006S18)*.

Hadiuzzaman, M., & Qiu, T. Z. (2013). Cell transmission model based variable speed limit control for freeways. *Canadian Journal of Civil Engineering*, 40, 46–56.

Hadiuzzaman, M., Qiu, T. Z., & Lu, X.-Y. (2012). Variable Speed Limit Control Design for Relieving Congestion Caused by Active Bottlenecks. *Journal of Transportation Engineering*, (April), 121006112354008. [https://doi.org/10.1061/\(ASCE\)TE.1943-5436.0000507](https://doi.org/10.1061/(ASCE)TE.1943-5436.0000507)

Han, Y., Chen, D., & Ahn, S. (2017). Variable speed limit control at fixed freeway bottlenecks using connected vehicles. *Transportation Research Part B: Methodological*, 98, 113–134. <https://doi.org/10.1016/j.trb.2016.12.013>

Hegyí, A., De Schutter, B., & Hellendoorn, H. (2005a). Model predictive control for optimal coordination of ramp metering and variable speed limits. *Transportation Research Part C: Emerging Technologies*, 13, 185–209. <https://doi.org/10.1016/j.trc.2004.08.001>

- Hegyi, A., De Schutter, B., & Hellendoorn, J. (2005b). Optimal coordination of variable speed limits to suppress shock waves. In *IEEE Transactions on Intelligent Transportation Systems* (Vol. 6, pp. 102–112). <https://doi.org/10.1109/TITS.2004.842408>
- Hegyi, A., & Hoogendoorn, S. P. (2010). Dynamic speed limit control to resolve shock waves on freeways - Field test results of the SPECIALIST algorithm. *IEEE Conference on Intelligent Transportation Systems, Proceedings, ITSC*, 519–524. <https://doi.org/10.1109/ITSC.2010.5624974>
- Hegyi, A., Hoogendoorn, S. P., Schreuder, M., Stoelhorst, H., & Viti, F. (2008). SPECIALIST: A dynamic speed limit control algorithm based on shock wave theory. *2008 11th International IEEE Conference on Intelligent Transportation Systems*, 827–832. <https://doi.org/10.1109/ITSC.2008.4732611>
- Jin, H., & Jin, W. (2013). Control of a lane-drop bottleneck through variable speed limits. *ArXiv Preprint ArXiv:1310.2658*, 1–31. <https://doi.org/10.1016/j.trc.2014.08.024>
- Jin, H. Y., & Jin, W. L. (2015). Control of a lane-drop bottleneck through variable speed limits. *Transportation Research Part C: Emerging Technologies*, 58, 568–584. <https://doi.org/10.1016/j.trc.2014.08.024>
- Kang, K.-P., Chang, G.-L., & Zou, N. (2004). Optimal Dynamic Speed-Limit Control for Highway Work Zone Operations. *Transportation Research Record*, 1877, 77–84. <https://doi.org/10.3141/1877-09>
- Khondaker, B., & Kattan, L. (2015a). Variable speed limit: A microscopic analysis in a

connected vehicle environment. *Transportation Research Part C: Emerging Technologies*, 58, 146–159. <https://doi.org/10.1016/j.trc.2015.07.014>

Khondaker, B., & Kattan, L. (2015b). Variable speed limit: an overview. *Transportation Letters*, 1942787514Y.000. <https://doi.org/10.1179/1942787514Y.0000000053>

Knoop, V. L., Duret, A., Buisson, C., & Van Arem, B. (2010). Lane distribution of traffic near merging zones influence of variable speed limits. In *IEEE Conference on Intelligent Transportation Systems, Proceedings, ITSC* (pp. 485–490). <https://doi.org/10.1109/ITSC.2010.5625034>

Lasdon, L. S., Fox, R. L., & Ratner, M. W. (1974). Nonlinear optimization using the generalized reduced gradient method. *RAIRO Operations Research*, 8, 73–103.

Lee, C., Hellinga, B., & Saccomanno, F. (2006). Evaluation of variable speed limits to improve traffic safety. *Transportation Research Part C: Emerging Technologies*, 14, 213–228. <https://doi.org/10.1016/j.trc.2006.06.002>

Lin, P.-W., Kang, K.-P., & Chang, G.-L. (2004). Exploring the Effectiveness of Variable Speed Limit Controls on Highway Work-Zone Operations. *Journal of Intelligent Transportation Systems*, 8(3), 155–168. <https://doi.org/10.1080/15472450490492851>

Lu, X.-Y., Qiu, T. Z., Varaiya, P., Horowitz, R., & Shladover, S. E. (2010). Combining Variable Speed Limits with Ramp Metering for Freeway Traffic Control. In *American Control Conference* (pp. 2266–2271).

Lu, X.-Y., Varaiya, P., Horowitz, R., Su, D., & Shladover, S. E. (2010). A new approach

for combined freeway Variable Speed Limits and Coordinated Ramp Metering. In *13th International IEEE Conference on Intelligent Transportation Systems* (pp. 491–498). <https://doi.org/10.1109/ITSC.2010.5625107>

Mitchell, T. M. (1997). *Machine Learning*. McGraw-Hill. <https://doi.org/10.1145/242224.242229>

Mizuta, A., Roberts, K., Jacobson, L., & Thompson, N. (2014). *Ramp Metering: A Proven, Cost-Effective Operational Strategy—A Primer*. U.S. Department of Transportation. Retrieved from <https://ops.fhwa.dot.gov/publications/fhwahop14020/sec1.htm>

Müller, E. R., Carlson, R. C., Kraus, W., & Papageorgiou, M. (2015). Microsimulation Analysis of Practical Aspects of Traffic Control With Variable Speed Limits, *16*(1), 512–523.

Papageorgiou, M., Hadj-Salem, H., & Blosseville, J.-M. (1990). ALINEA: a local feedback control law for on ramp metering. *Transportation Research Record 1320*, 58–64.

Papageorgiou, M., Hadj-Salem, H., & Middelham, F. (1997). ALINEA Local Ramp Metering: Summary of Field Results. *Transportation Research Record, 1603*(1), 90–98. <https://doi.org/10.3141/1603-12>

Papageorgiou, M., Kosmatopoulos, E., & Papamichail, I. (2008). Effects of Variable Speed Limits on Motorway Traffic Flow. *Transportation Research Board, 2047*, 37–48. <https://doi.org/10.3141/2047-05>

- Papageorgiou, M., & Kotsialos, A. (2002). Freeway ramp metering: An overview. *IEEE Transactions on Intelligent Transportation Systems*, 3(4), 271–281.
- Schelling, I., Hegyi, A., & Hoogendoorn, S. P. (2011). SPECIALIST-RM - Integrated variable speed limit control and ramp metering based on shock wave theory. In *IEEE Conference on Intelligent Transportation Systems, Proceedings, ITSC* (pp. 2154–2159). <https://doi.org/10.1109/ITSC.2011.6083116>
- Smulders, S. (1990). Control of freeway traffic flow by variable speed signs. *Transportation Research Part B: Methodological*, 24, 111–132. [https://doi.org/10.1016/0191-2615\(90\)90023-R](https://doi.org/10.1016/0191-2615(90)90023-R)
- Soriguera, F., Martinez, I., Sala, M., & Menendez, M. (2017). Effects of low speed limits on freeway traffic flow. *Transportation Research Part C: Emerging Technologies*, 77, 257–274. <https://doi.org/10.1016/j.trc.2017.01.024>
- Talebpour, A., Mahmassani, H. S., & Hamdar, S. H. (2013). Speed Harmonization. *Transportation Research Record: Journal of the Transportation Research Board*, 2391, 69–79. <https://doi.org/10.3141/2391-07>
- Yang, H., & Rakha, H. (2017). Feedback control speed harmonization algorithm: Methodology and preliminary testing. *Transportation Research Part C*, 81, 209–226.

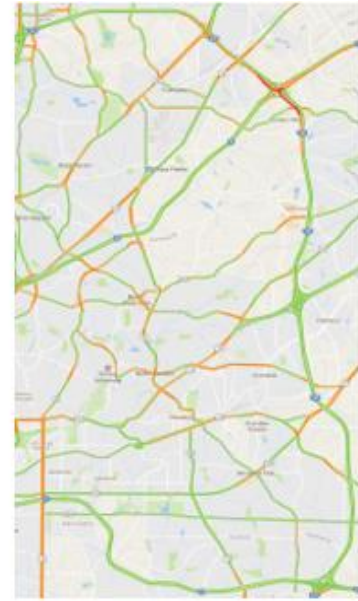
9. Appendix



(a) 2016 4/4 2:30



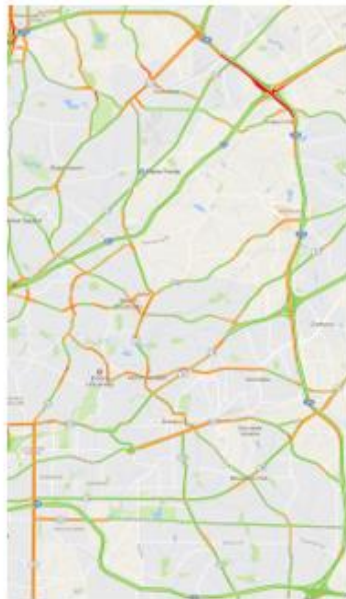
(b) 2016 4/4 2:45



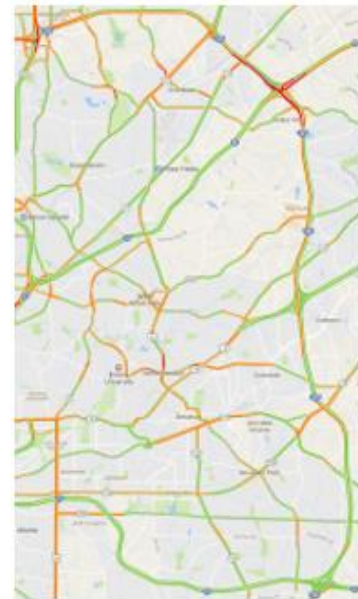
(c) 2016 4/4 2:45



(d) 2016 4/4 3:15



(e) 2016 4/4 3:30

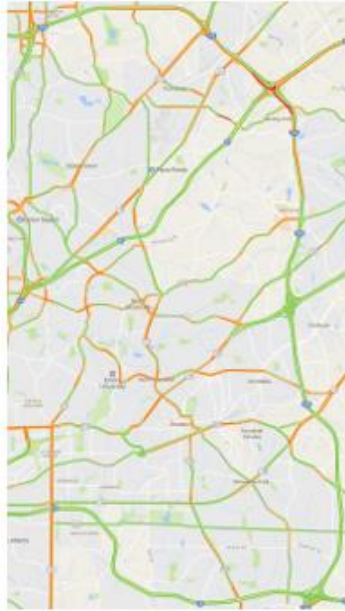


(f) 2016 4/4 3:45

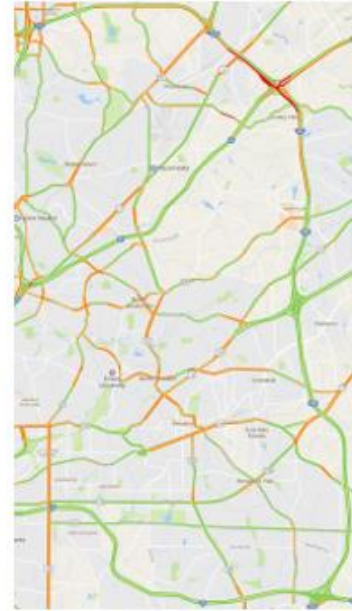
Figure 37 Typical Traffic State on I-285 Corridor on Monday PM Peak



(a) 2016 4/5 2:30



(b) 2016 4/5 2:45



(c) 2016 4/5 2:45



(d) 2016 4/5 3:15



(e) 2016 4/5 3:30



(f) 2016 4/5 3:45

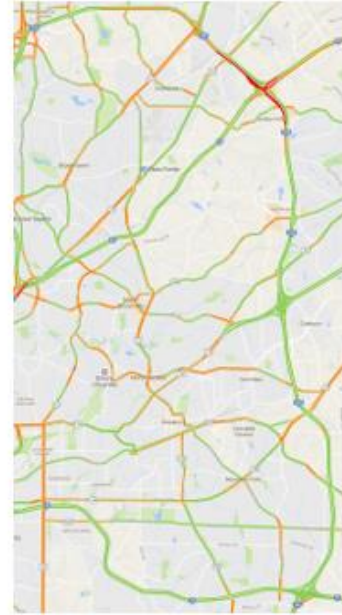
Figure 38 Typical Traffic State on I-285 Corridor on Tuesday PM Peak



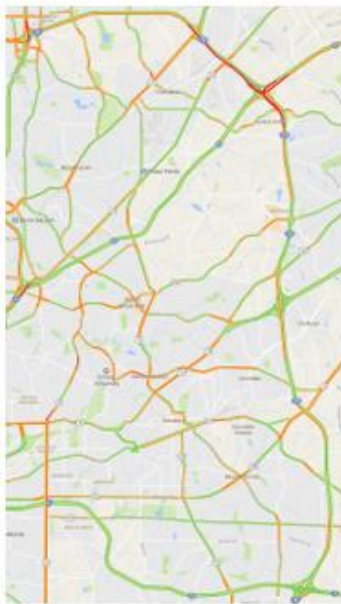
(a) 2016 4/6 2:30



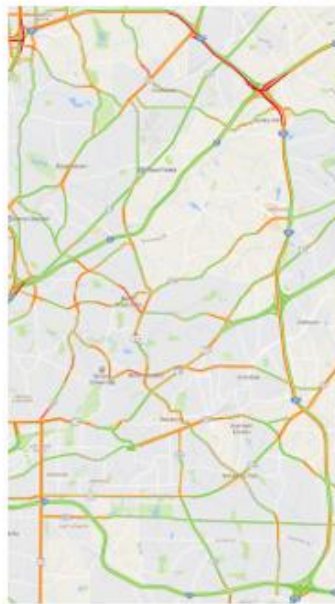
(b) 2016 4/6 2:45



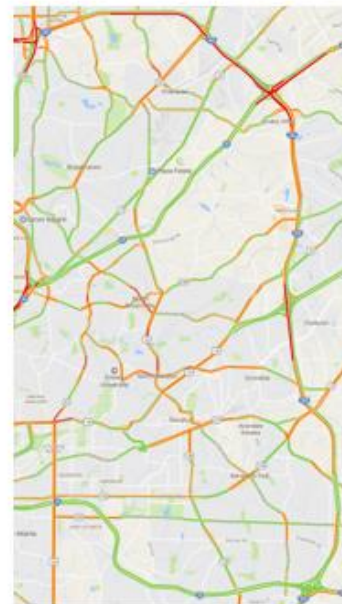
(c) 2016 4/6 2:45



(d) 2016 4/6 3:15



(e) 2016 4/6 3:30

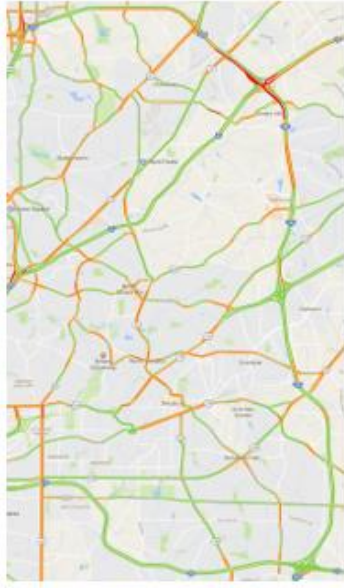


(f) 2016 4/6 3:45

Figure 39 Typical Traffic State on I-285 Corridor on Wednesday PM Peak



(a) 2016 4/7 2:30



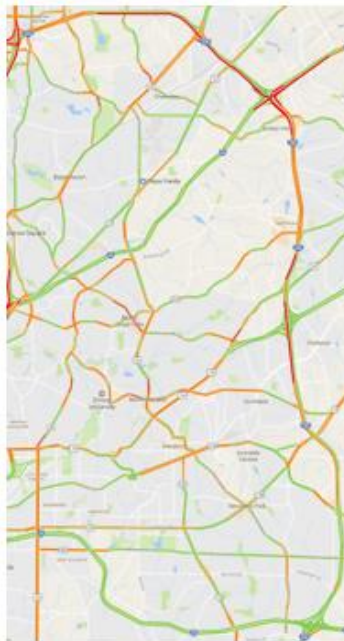
(b) 2016 4/7 2:45



(c) 2016 4/7 2:45



(d) 2016 4/7 3:15



(e) 2016 4/7 3:30

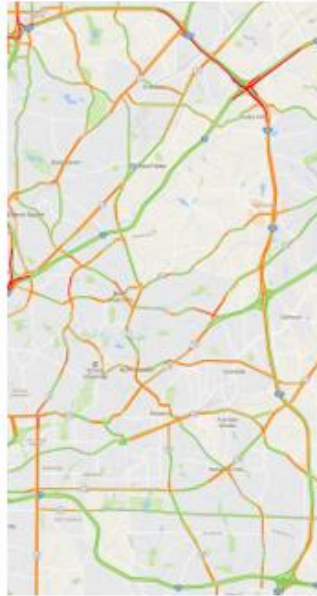


(f) 2016 4/7 3:45

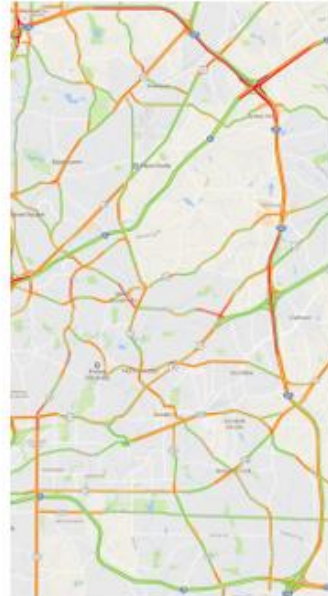
Figure 40 Typical Traffic State on I-285 Corridor on Thursday PM Peak



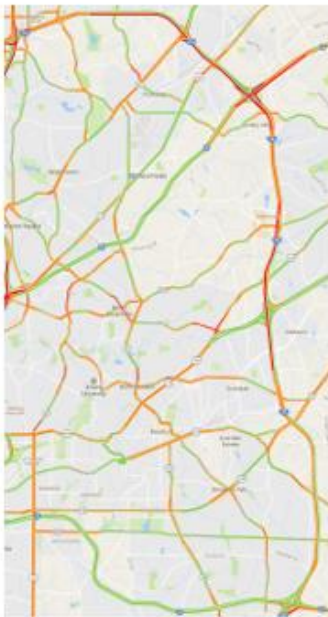
(a) 2016 4/8 2:30



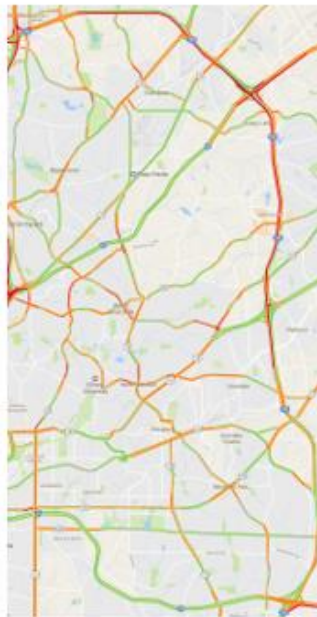
(b) 2016 4/8 2:45



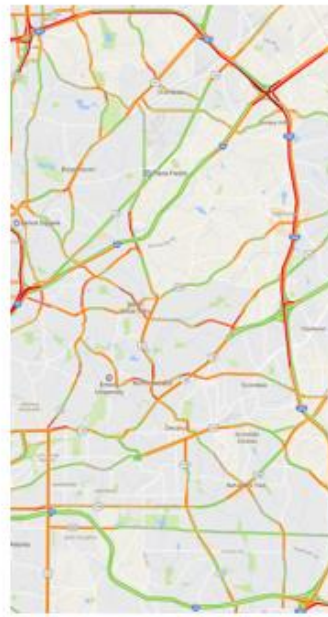
(c) 2016 4/8 2:45



(d) 2016 4/8 3:15

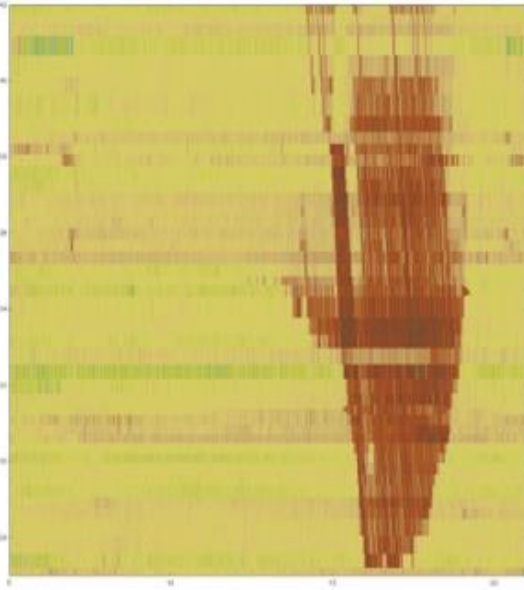


(e) 2016 4/8 3:30

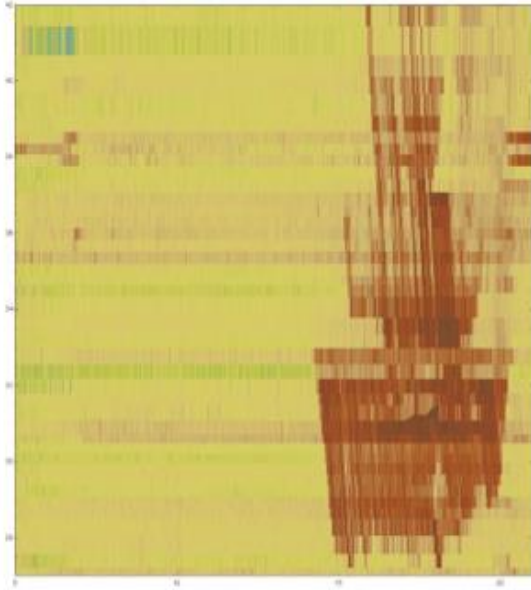


(f) 2016 4/8 3:45

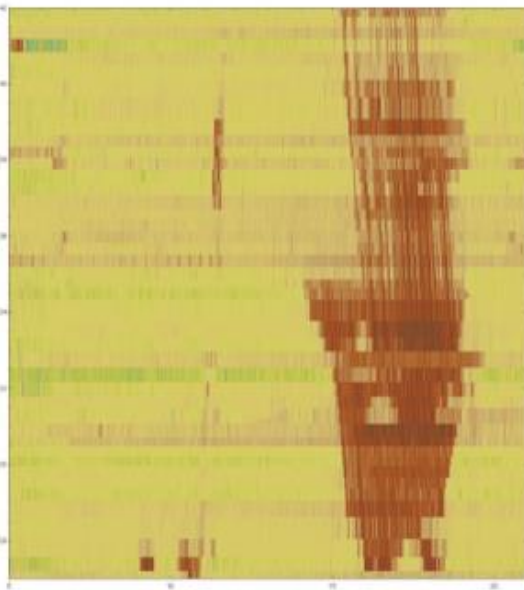
Figure 41 Typical Traffic State on I-285 Corridor on Friday PM Peak



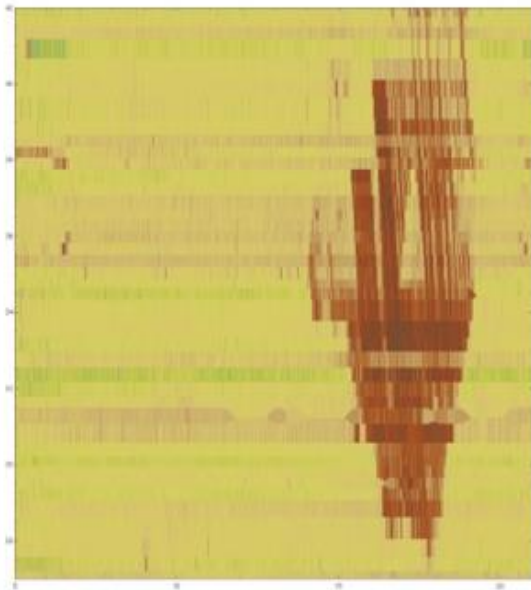
(a) 2016/04/04



(b) 2016/04/11

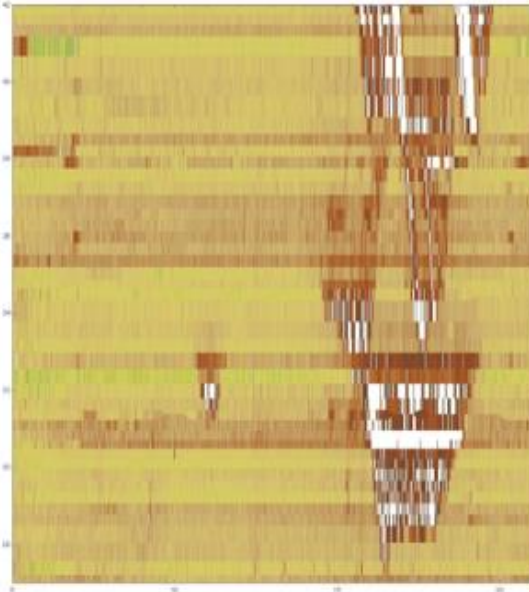


(c) 2016/04/18

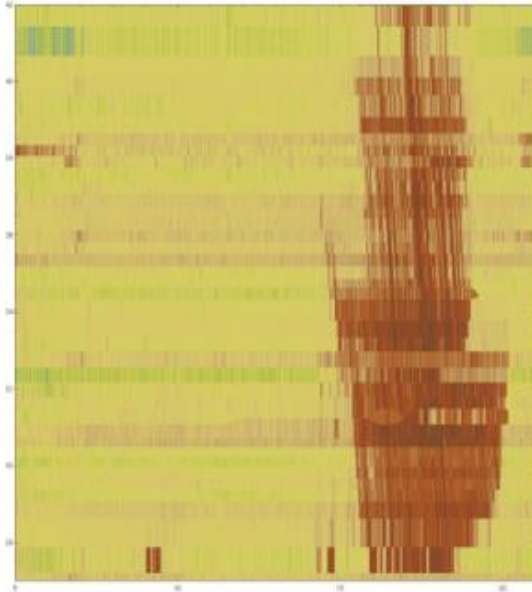


(d) 2016/04/25

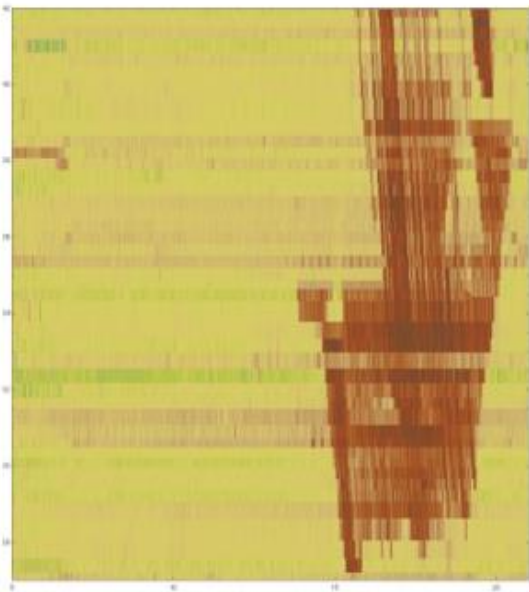
Figure 42 April 2016 Monday Traffic. Low-speed regions are in brown and high-speed regions are in yellow.



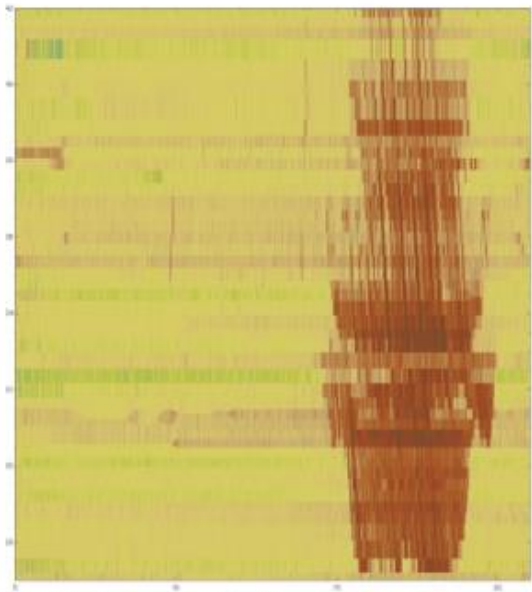
(a) 2016/04/05



(b) 2016/04/12

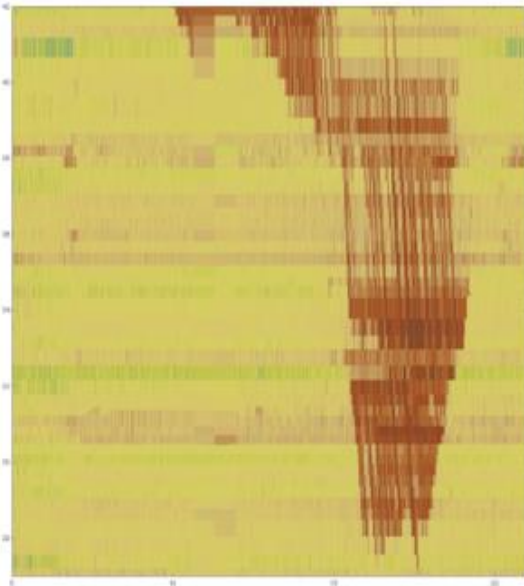


(c) 2016/04/19

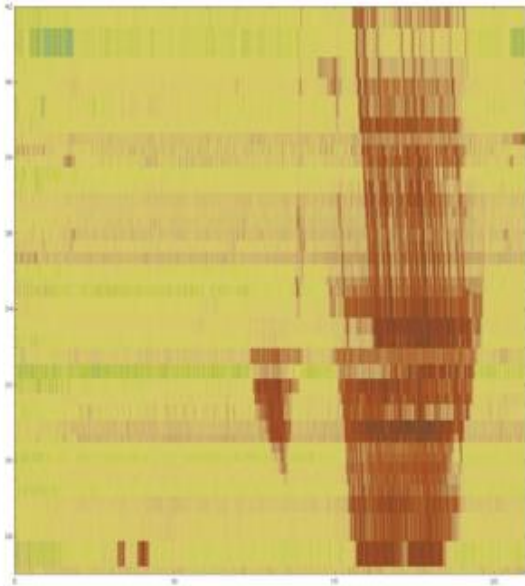


(d) 2016/04/26

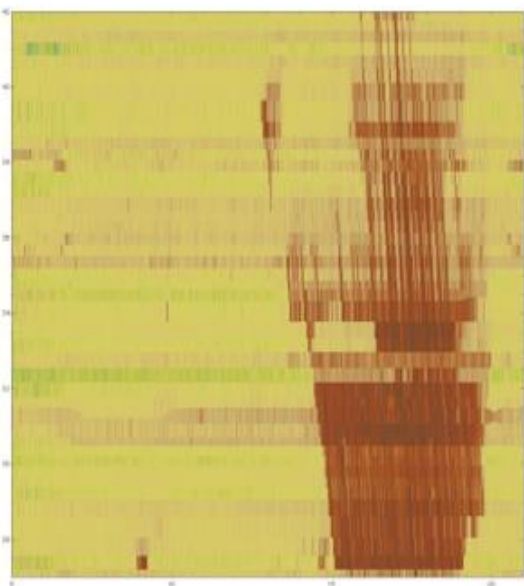
Figure 43 April 2016 Tuesday Traffic. Low-speed regions are in brown and high-speed regions are in yellow.



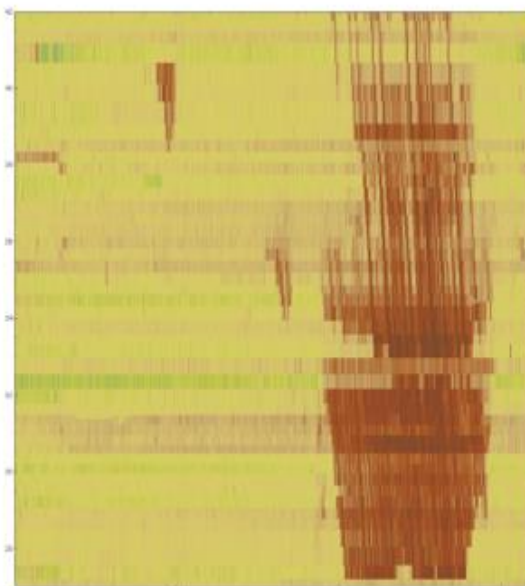
(a) 2016/04/06



(b) 2016/04/13

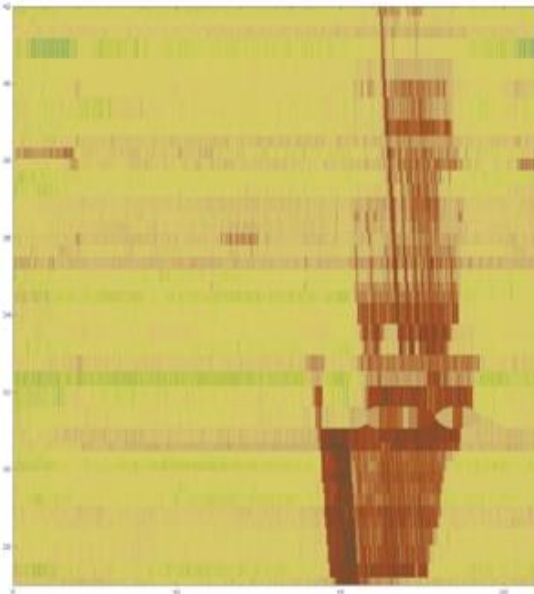


(c) 2016/04/20

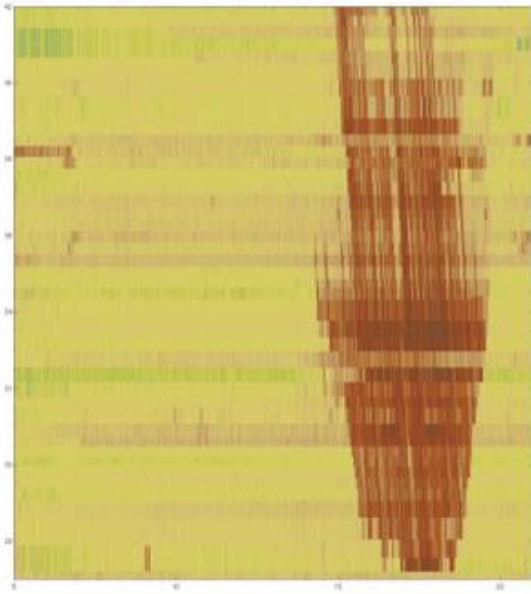


(d) 2016/04/27

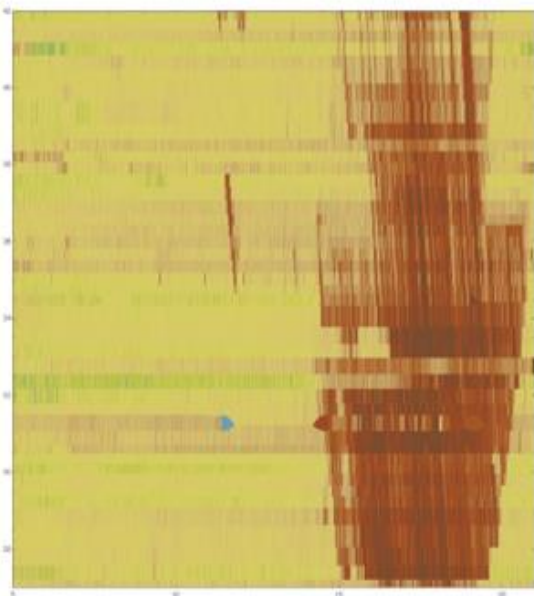
Figure 44 April 2016 Wednesday Traffic. Low-speed regions are in brown and high-speed regions are in yellow.



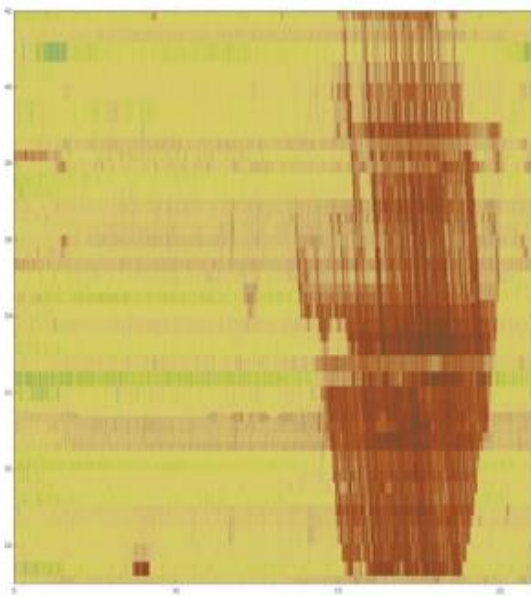
(a) 2016/04/07



(b) 2016/04/14

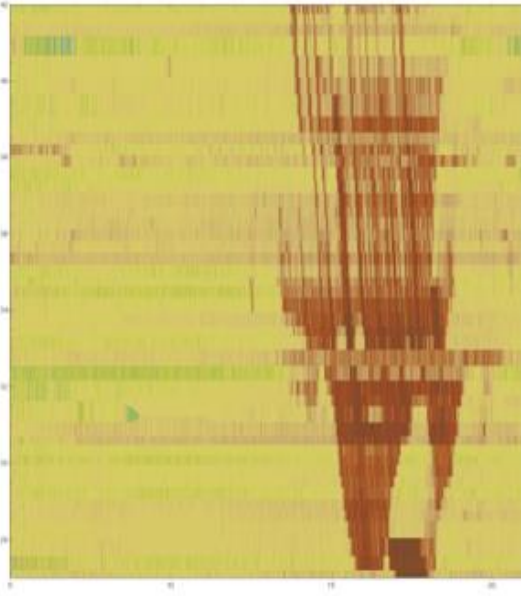


(c) 2016/04/21

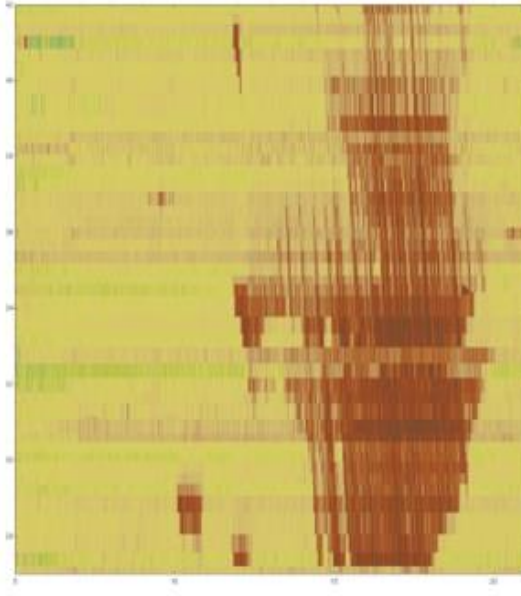


(d) 2016/04/28

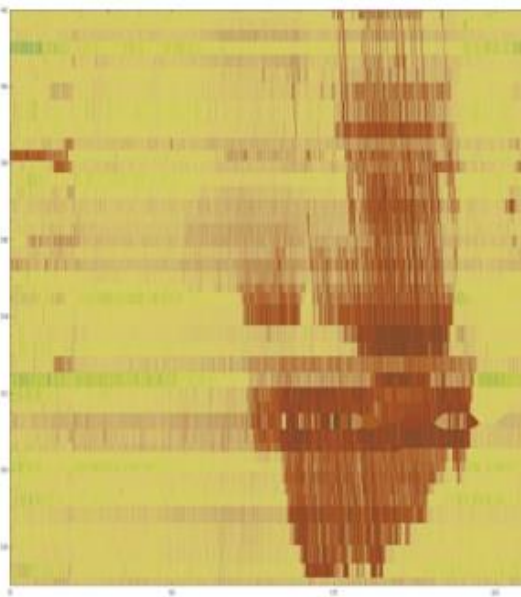
Figure 45 April 2016 Thursday Traffic. Low-speed regions are in brown and high-speed regions are in yellow.



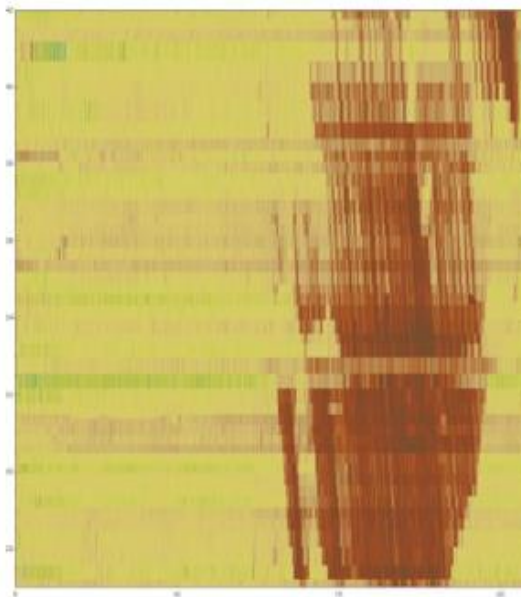
(a) 2016/04/08



(b) 2016/04/15



(c) 2016/04/22



(d) 2016/04/29

Figure 46 April 2016 Friday Traffic. Low-speed regions are in brown and high-speed regions are in yellow.